DOKUZ EYLÜL UNIVERSITY

GRADUATE SCHOOL OF NATURAL AND APPLIED SCIENCES

STRENGTH PREDICTION OF PIN-LOADED LAMINATED COMPOSITE PLATES

by

Cihan Rıza ÇALIŞKAN

July, 2005

İZMİR

STRENGTH PREDICTION OF PIN-LOADED LAMINATED COMPOSITE PLATES

A Thesis Submitted to the
Graduate School and Applied Sciences of Dokuz Eylül University
In Partial Fulfillment of the Requirements for the Degree of Master of Science
in Mechanical Engineering, Mechanics Program

by

Cihan Rıza ÇALIŞKAN

July, 2005
İZMİR

Ms. Sc. THESIS EXAMINATION RESULT FORM

We have read the thesis, entitled **"STRENGTH PREDICTION OF PIN-LOADED LAMINATED COMPOSITE PLATES"** completed by **CİHAN RIZA ÇALIŞKAN** under supervision of **Prof. Dr. RAMAZAN KARAKUZU** and we certify that in our opinion it is fully adequate, in scope and in quality, as a thesis for the degree of Master of Science.

Prof. Dr. Ramazan Karakuzu

Supervisor

(Committee Member)

(Committee Member)

Prof. Dr. Cahit Helvacı
Director
Graduate School of Natural and Applied Sciences

ACKNOWLEDGEMENTS

I would like to express to my sincere gratitude to Prof. Dr. Ramazan KARAKUZU, for his supervision, valuable guidance and continuous encouragement throughout this study.

I want to express my thanks to the research assistants, B.Murat ICTEN, Mehmet AKTAŞ and Yusuf ARMAN at Dokuz Eylul Universty for their great help during my study.

I thank personal of Izoreel Firm for manufacture of the glass-vinylester composite plates. Thanks goes out to the technician, Ahmet YİĞİT, in the Machine Tool Laboratory and special thanks to Tayfun GÜLEM and Aydoğan SİPAHİ, for their help during this study.

Finally, I wish to express sincere thanks to my family for their moral support, patience and understanding while preparing this thesis.

Cihan Rıza ÇALIŞKAN

STRENGTH PREDICTION OF PIN-LOADED LAMINATED COMPOSITE PLATES

ABSTRACT

In this study, behaviour of pin-loaded laminated composite plates with different dimensions have been observed numerically and experimentally. The aim is to investigate bearing strength, failure load and failure mode in a laminated glass-vinylester composite plate with two circular holes in series. The holes of the plate are subjected to a traction force by two rigid pins.

These are investigated for three variables; the hole is a distance from the free edge of the plate of width-to-hole of diameter (E/D) ratio (1,2,3,4,5), rectangular plate of width-to-hole of diameter W/D ratio (2,3,4,5) and the distance between two holes to diameter K/D ratio (2,3,4,5). Orientation angle of fiber $\theta = 0°$ is constant in numerical and experimental study. The failure analysis is performed numerically and experimentally for eighty different geometries.

Three dimensional finite element method is used for numerical study. Numerical study is performed with assistance of LUSAS 13.3 finite element analysis program. In this program, maximum failure load is found with nonlinear analysis, Hashin failure criteria is used in this failure analysis. In the case of failure, appropriate properties of the nodes failed of the composite plate are reduced.

Failure types on the specimens are predicted and maximum failure loads are found in experimental study.

The results of experimental study and numerical study are compared and quite reasonable. Bearing strength which is depending on applied force and dimensions of the plate are shown in graphs.

Keywords : Pin, failure analysis, bearing strength, laminated composite.

PİM YÜKÜ ETKİSİ ALTINDAKİ TABAKALI KOMPOZİT PLAĞIN MUKAVEMETİNİN BELİRLENMESİ

ÖZ

Bu çalışmada, farklı boyutlara sahip tabakalı kompozitlerin, pim yükü etkisi altındaki davranışları, nümerik ve deneysel olarak incelenmiştir. Amaç, çift pim bağlantılı tabakalı glass-vinylester kompozit plağın, yırtılma mukavemetini, hasar yükünü ve hasar modunu tespit etmektir. Plakanın delikleri rigid iki pim yardımıyla değişken yayılı yüke maruz bırakılmıştır.

Bu çalışmalar, plakanın uç kısmının deliğin çapına oranı; birden beşe kadar, plakanın genişliğinin deliğin çapına oranı; ikiden beşe kadar ve delikler arası uzaklığın deliğin çapına oranı; ikiden beşe kadar, üç farklı şekilde araştırılmıştır. Deneysel ve nümerik çalışmalarda fiber yönlendirme açısı sabittir. Hasar analizi, seksen farklı geometri için incelenmiştir.

Nümerik çalışmada üç boyutlu sonlu eleman yöntemi kullanılmıştır. Nümerik çalışma LUSAS 13.3 sonlu eleman paket programı yardımıyla hazırlanmıştır. Bu programda maksimum hasar yükü nonlinear analiz yöntemiyle bulundu ve hasar analizinde Hashin kriteri kullanıldı. Hasar durumunda, kompozit plağın hasarlı düğümlerindeki malzeme özellikleri indirgendi.

Deneysel çalışmada, numuneler üzerindeki hasar tipleri belirlendi ve maksimum hasar yükleri bulundu.

Deneysel çalışma ve nümerik çalışma sonuçları karşılaştırılmış ve uygunluk içinde olduğu görülmüştür. Yırtılma mukavemeti kuvvet ve boyutlara bağlı olarak grafiklerle gösterilmiştir.

Anahtar sözcükler : Pim, hasar analizi, yırtılma mukavemeti, tabakalı kompozit.

CONTENTS

Page

NOMENCLATURE

Abbreviation	Term
D	Hole diameter
E	End distance from the hole center
W	Width of the plate
K	Distance between two holes
t	Thickness of the plate
L	Distance from hole center to fixed end
a, b, c, t_i	Dimensions of Iosipescu testing specimen
P	Tensile load
P_{ult}	Maximum failure load
θ	Fiber orientation angle
E_{ij}	Elastic moduli in material directions
G_{ij}	Shear moduli
ν_{12}	Poisson's ratio
V_f	Fiber volume friction
σ_b	Bearing strength
X_t	Tensile strength in the fiber direction
X_c	Compressive strength in the fiber direction
Y_t	Tensile strength in the transverse direction
Y_c	Compressive strength in the transverse direction
S	Shearing strength
ε_{ij}	Strains
σ_{ij}	Stresses
$[\overline{C}_{ij}]$	Reduced-stiffness matrix
$[C_{ij}]$	Inverse of compliance matrix
$[S_{ij}]$	Compliance matrix
u, v, w	Displacement components

CHAPTER ONE
INTRODUCTION

Composite materials are extensively used in structures that demand a high level of mechanical performance. Their high strength to weight and stiffness to weight ratios have facilitated the development of lighter structures, which often replace conventional metal structures. Due to strength and safety requirements, these applications require joining composites either to composites or to metals. Although leading to a weight penalty due to stress concentration created by drilling a hole in the laminate, mechanical fasteners are widely used in the aerospace industry. In fact mechanically fastened joints (such as pinned joints) are unavoidable in complex structures because of their low cost, simplicity for assemble and facilitation of disassembly for repair.

An unskillful design of joints in the case of mechanical fasteners often causes a reduction of load capability of the composite structure even though the composite materials posses high strength. Thus many papers on mechanical joints and specifically pin-loaded holes have been conducted in the past.

The numerical investigations of stress distributions in multi-pin joints have been found in literature. Both lines (parallel to the load) and rows (perpendicular to the load) of fasteners have been considered. Chang et al. (1984)a have extended their analysis to T300/1034-C laminates containing a pin-loaded hole or two pin- loaded holes in parallel or in series. Chang et al. (1984)b have developed a model and corresponding computer code to determine failure strength and failure mode of composite laminates containing a pin loaded hole even when the material exhibits nonlinearly elastic behaviour. Hassan et al. (1996) used a three-dimensional finite element model to perform stress analysis of single and multi-bolted double shear lap connections of glass-fiber reinforced plastic using ANSYS program. Kim and Kim (1995) have investigated two bolts in a line and in a row. Using extended interior penalty methods, variational formulation has been discretized using the finite element method. Contact clearances between pins and holes, geometric factors and

the load quantity have been considered as design parameters for three lamination angles. Using the same method, Kim et al. (1998) have carried out a progressive failure analysis to predict the failure strength and modes of pin-loaded composite. Mc Carthy et al. (2005) have investigated progressive damage analysis of multi-bolt composite joints with variable bolt-hole clearances using ABAQUS program.

Review papers on the strength of mechanically fastened joints in fiber-reinforced plastics have been written by Godwin & Matthews (1980) and Camanho & Matthews (1997). Effects of material properties, fastener parameters and design parameters have been summarized and discussed. These parameters are very important for the strength of mechanically joints in composite laminate.

Chang et al. (1982) have developed a computer code, which can be used to calculate the maximum load and the mode of joints involving fiber reinforced laminates with different ply orientation, different material properties, and different geometries. They have used Yamada failure criterion.

Aktas & Karakuzu (1999) have carried out failure analysis of mechanically fastened carbon fiber reinforced epoxy composite plate of arbitrary orientation. In that work, failure load and failure mode have been analysed experimentally and numerically using Tsai- Hill and fiber tensile-compressive failure criteria. Icten & Sayman (2003) have investigated failure load and failure mode in an aluminium-glass-epoxy sandwich composite plate, with a circular hole, which is subjected to a traction force by a pin. To evaluate the effects of joint geometry and fiber orientation on the failure strength and failure mode, parametric studies were performed experimentally. Icten et al. (2002) have investigated mechanical behaviour and damage development of pin-loaded woven glass fiber-epoxy composites, numerically and experimentally. To verify to the numerical predictions of mechanical behaviour, a series of material configurations ($[(0/90)_3]_S$-$[(\pm45)_3]_S$) and twenty different geometries. Icten & Karakuzu (2002) have concerned with the prediction and examination of the behaviours of the pinned joint carbon-epoxy composite plates. The failure mode and bearing strength have been investigated numerically and

experimentally. The two-dimensional finite element method has been used to determine the failure load and failure mode using Hoffman and Hashin criteria. The mechanical properties of the composite material have been obtained from standard tests. Okutan, Aslan and Karakuzu (2001) have studied the effects of woven fiber, specimen width-to-hole diameter (W/D) and the ratio of edge distance to hole diameter (E/D) on the bearing strength of woven laminated composites. They have tested single-hole pin-loaded specimens for their tensile response. They have observed failure propagation and failure type on the specimens. Okutan et al. (2001) have investigated the failure strength of pin-loaded woven fiber-glass reinforced epoxy laminates experimentally and have observed the effects of changing the geometric parameters were observed.

Okutan & Karakuzu (2002) have investigated the bearing strength and failure mechanisms of pinned joints in laminated composites. For this purpose, the specimens have been tested to find first failure and final failure load. In addition, they have performed a static progressive failure analysis by using finite element code PDNLPIN.

Chang (1986) has performed an analysis to evaluate the effect of the assumed pin load distribution. The calculations have utilized a finite element method of stress analysis combined with the Yamada-Sun failure criterion applied along the Chang-Scott- Springer characteristic curve. Hung et al. (1996) have investigated failure analysis of T800/3900-2 graphite-epoxy materials by using Hashin failure criteria. Camanho & Matthews (1999) have developed a 3D finite element model to predict damage progression and strength of mechanically fastened joints in carbon-fibre reinforced plastics. To predict the failure mode, Hashin failure criteria has been used and compared with the experimental results.

Lessard and Shokrieh (1995) have used two-dimensional linear and non-linear models to predict the strengths of pin-loaded holes. In the linear model five types of failure have been considered. Matrix tensile and compressive failure, fiber/matrix shearing and fiber tensile and compressive failure have been predicted using Hashin

failure criterion. Pierron & Cerisier (2000) have carried out a numerical and experimental study to determine the stiffness and the bearing strength of bolted woven composite joints. In addition, they have studied for the influence of the clearance. Hamada & Maekawa (1996) have examined failure analysis of quasi-isotropic carbon epoxy T300/#2500 laminates numerically and experimentally. Dano et al. (2000) have determined the deformation behavior of the pin-loaded joint using a two-dimensional finite element model developed in the commercial software ABAQUS. Pierron et al. (2000) have used ABAQUS in order to calculate stress distribution around the hole of woven composite joint.

Several authors have highlighted the importance of width (W), end distance (E), hole diameter (D) and laminate thickness (t) on the joint strength. Kretsis & Matthews (1985) showed, using E glass fiber-reinforced plastic and carbon fiber-reinforced plastic, that as the width of the specimen decreases, there is a point where the made of failure changes from one of bearing to one of tension. A similar behaviour between the end distance and the shear-out mode of failure was found. They concluded that lay-up had a great effect on both joint strength and failure mechanism.

In this study, the failure mode, failure load and bearing strength are investigated in glass-vinylester laminated composite plate containing two pin-loaded holes in series numerically and experimentally. The effects of changing the geometric parameters are observed. The three-dimensional finite element method is used to determine the failure load and failure mode using Hashin criteria.

CHAPTER TWO
STRESS AND FAILURE ANALYSIS

2.1 Stress Analysis

In this chapter, information is given about macromechanical behavior of lamina and laminate. The purpose of a joint is to transfer load between the two parts being joined. As a result of this load transfer there will be a stress variation in the components in the joint region. In most cases, an accurate understanding of the stress distributions in the joint is one of the critical ingredients. Although other methods of analysis may identify the origin and mode of failure, stress analysis most often provides a quantitative explanation for the cause of failure. Stress analysis procedures for composite materials are complex. In order to utilize the full potential of the specific strength of composite materials, accurate stress distributions must be known.

2.1.1 Stress-Strain Relations in an Orthotropic Material

For an orthotropic material, three dimensional strain-stress relations can be written as:

$$\begin{Bmatrix} \varepsilon_1 \\ \varepsilon_2 \\ \varepsilon_3 \\ \gamma_{23} \\ \gamma_{31} \\ \gamma_{12} \end{Bmatrix} = \begin{bmatrix} S_{11} & S_{12} & S_{13} & 0 & 0 & 0 \\ S_{12} & S_{22} & S_{23} & 0 & 0 & 0 \\ S_{13} & S_{23} & S_{33} & 0 & 0 & 0 \\ 0 & 0 & 0 & S_{44} & 0 & 0 \\ 0 & 0 & 0 & 0 & S_{55} & 0 \\ 0 & 0 & 0 & 0 & 0 & S_{66} \end{bmatrix} \begin{Bmatrix} \sigma_1 \\ \sigma_2 \\ \sigma_3 \\ \tau_{23} \\ \tau_{31} \\ \tau_{12} \end{Bmatrix} \tag{2.1}$$

where

$$S_{11} = \frac{1}{E_1}, \quad S_{12} = -\frac{\nu_{12}}{E_1} = -\frac{\nu_{21}}{E_2}, \quad S_{13} = -\frac{\nu_{13}}{E_1} = -\frac{\nu_{31}}{E_3}, \quad S_{23} = -\frac{\nu_{23}}{E_2} = -\frac{\nu_{32}}{E_3}$$

$$S_{22} = \frac{1}{E_2}, \quad S_{33} = \frac{1}{E_3}, \quad S_{44} = \frac{1}{G_{23}}, \quad S_{55} = \frac{1}{G_{31}}, \quad S_{66} = \frac{1}{G_{12}} \tag{2.2}$$

By assuming three dimensional orthotropic material properties for each unidirectional ply, the number of material properties reduced nine. A unidirectional ply is shown in Figure 2.1.

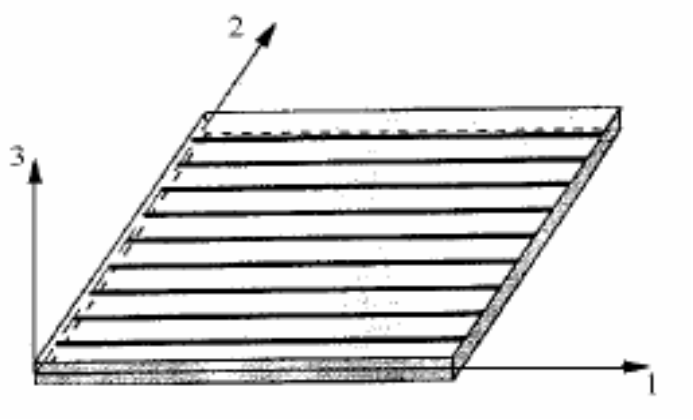

Figure 2.1 A unidirectional fiber reinforced lamina

The strain-stress relations in Eq. 2.1 can be inverted to obtain the stress-strain relations:

$$\begin{Bmatrix} \sigma_1 \\ \sigma_2 \\ \sigma_3 \\ \tau_{23} \\ \tau_{31} \\ \tau_{12} \end{Bmatrix} = \begin{bmatrix} C_{11} & C_{12} & C_{13} & 0 & 0 & 0 \\ C_{12} & C_{22} & C_{23} & 0 & 0 & 0 \\ C_{13} & C_{23} & C_{33} & 0 & 0 & 0 \\ 0 & 0 & 0 & C_{44} & 0 & 0 \\ 0 & 0 & 0 & 0 & C_{55} & 0 \\ 0 & 0 & 0 & 0 & 0 & C_{66} \end{bmatrix} \begin{Bmatrix} \varepsilon_1 \\ \varepsilon_2 \\ \varepsilon_3 \\ \gamma_{23} \\ \gamma_{31} \\ \gamma_{12} \end{Bmatrix} \tag{2.3}$$

The stiffness matrix, C_{ij}, for an orthotropic materials in terms of the engineering constants, is obtained by inversion of the compliance matrix, S_{ij}. The stiffnesses in Eq. (2.3) are,

$$C_{11} = \frac{1-\nu_{23}\nu_{32}}{E_2 E_3 \Delta}, \qquad C_{22} = \frac{1-\nu_{13}\nu_{31}}{E_1 E_3 \Delta}, \qquad C_{12} = \frac{\nu_{21}+\nu_{31}\nu_{23}}{E_2 E_3 \Delta} = \frac{\nu_{12}+\nu_{32}\nu_{13}}{E_1 E_3 \Delta},$$

$$C_{23} = \frac{\nu_{32}+\nu_{12}\nu_{31}}{E_1 E_3 \Delta} = \frac{\nu_{23}+\nu_{21}\nu_{13}}{E_1 E_2 \Delta}, \qquad C_{13} = \frac{\nu_{31}+\nu_{21}\nu_{32}}{E_2 E_3 \Delta} = \frac{\nu_{13}+\nu_{12}\nu_{23}}{E_1 E_2 \Delta},$$

$$C_{33} = \frac{1-\nu_{12}\nu_{21}}{E_1 E_2 \Delta}, \qquad C_{44} = G_{23}, \qquad C_{55} = G_{31}, \qquad C_{66} = G_{12} \tag{2.4}$$

where

$$\Delta = \frac{1-\nu_{12}\nu_{21}-\nu_{23}\nu_{32}-\nu_{31}\nu_{13}-2\nu_{21}\nu_{32}\nu_{13}}{E_1 E_2 E_3} \tag{2.5}$$

2.1.2 Stress-Strain Relations for a Lamina of Arbitrary Orientation

The reduced stiffness and compliance matrices relate stresses and strains in the principal material directions of the material. To define the material response in directions other than these material coordinates, transformation matrices must be developed for the material stiffness. In Figure 3.2, two sets of cordinate system are shown.

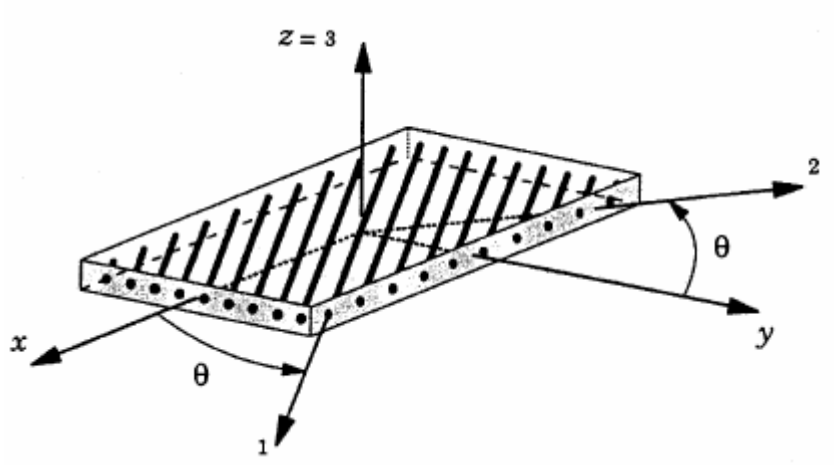

Figure 2.2 A fiber - reinforced lamina with global and material coordinate system

The 1-2-3 coordinate system corresponds to the principal material directions for a lamina, while the x-y-z coordinates are arbitrary and are related to the 1-2-3 coordinates through a rotation about the axis out of the plane of the Figure 3.2. The angle, θ, is defined as the rotation from the arbitrary x-y-z system to the material 1-2-3 system.

The transformation of stresses from the 1-2-3 system to the x-y-z system is,

$$\begin{Bmatrix}\sigma_x\\ \sigma_y\\ \sigma_z\\ \tau_{yz}\\ \tau_{xz}\\ \tau_{xy}\end{Bmatrix}=\begin{bmatrix}\cos^2\theta & \sin^2\theta & 0 & 0 & 0 & -\sin 2\theta\\ \sin^2\theta & \cos^2\theta & 0 & 0 & 0 & \sin 2\theta\\ 0 & 0 & 1 & 0 & 0 & 0\\ 0 & 0 & 0 & \cos\theta & \sin\theta & 0\\ 0 & 0 & 0 & -\sin\theta & \cos\theta & 0\\ \sin\theta\cos\theta & -\sin\theta\cos\theta & 0 & 0 & 0 & \cos^2\theta-\sin^2\theta\end{bmatrix}\begin{Bmatrix}\sigma_1\\ \sigma_2\\ \sigma_3\\ \tau_{23}\\ \tau_{31}\\ \tau_{12}\end{Bmatrix} \quad (2.6)$$

The strain-stress relations in x-y-z coordinates are,

$$\begin{Bmatrix}\varepsilon_x\\ \varepsilon_y\\ \varepsilon_z\\ \gamma_{yz}\\ \gamma_{xz}\\ \gamma_{xy}\end{Bmatrix}=\begin{bmatrix}\overline{S}_{11} & \overline{S}_{12} & \overline{S}_{13} & 0 & 0 & \overline{S}_{16}\\ \overline{S}_{21} & \overline{S}_{22} & \overline{S}_{13} & 0 & 0 & \overline{S}_{26}\\ \overline{S}_{31} & \overline{S}_{32} & \overline{S}_{33} & 0 & 0 & \overline{S}_{36}\\ 0 & 0 & 0 & \overline{S}_{44} & \overline{S}_{45} & 0\\ 0 & 0 & 0 & \overline{S}_{45} & \overline{S}_{55} & 0\\ \overline{S}_{16} & \overline{S}_{26} & \overline{S}_{36} & 0 & 0 & \overline{S}_{66}\end{bmatrix}\begin{Bmatrix}\sigma_x\\ \sigma_y\\ \sigma_z\\ \tau_{yz}\\ \tau_{xz}\\ \tau_{xy}\end{Bmatrix} \quad (2.7)$$

The transformed compliance coefficients $\overline{S}_{ij}$, referred to the (x, y, z) system,

$$\overline{S}_{11} = S_{11}\cos^4\theta - 2S_{16}\cos^3\theta\sin\theta + (2S_{12}+S_{66})\cos^2\theta\sin^2\theta - 2S_{26}\cos\theta\sin^3\theta + S_{22}\sin^4\theta$$

$$\overline{S}_{12} = S_{12}\cos^4\theta + (S_{16}-S_{26})\cos^3\theta\sin\theta + (S_{11}+S_{22}-S_{66})\cos^2\theta\sin^2\theta + (S_{26}-S_{16})\cos\theta\sin^3\theta + S_{12}\sin^4\theta$$

$$\overline{S}_{13} = S_{13}\cos^2\theta - S_{36}\cos\theta\sin\theta + S_{23}\sin^2\theta$$

$$\overline{S}_{16} = S_{16}\cos^4\theta + (2S_{11}-2S_{12}-S_{66})\cos^3\theta\sin\theta + 3(S_{26}-S_{16})\cos^2\theta\sin^2\theta + (S_{66}+2S_{12}-2S_{22})\cos\theta\sin^3\theta - S_{26}\sin^4\theta$$

$$\overline{S}_{22} = S_{22}\cos^4\theta + 2S_{26}\cos^3\theta\sin\theta + (2S_{12}+S_{66})\cos^2\theta\sin^2\theta + 2S_{16}\cos\theta\sin^3\theta + S_{11}\sin^4\theta$$

$$\overline{S}_{23} = S_{23}\cos^2\theta + S_{36}\cos\theta\sin\theta + S_{13}\sin^2\theta$$

$$\overline{S}_{26} = S_{26}\cos^4\theta + (2S_{12} - 2S_{22} + S_{66})\cos^3\theta\sin\theta + 3(S_{16} - S_{26})\cos^2\theta\sin^2\theta + (2S_{11} - 2S_{12} - S_{66})\cos\theta\sin^3\theta - S_{16}\sin^4\theta$$

$$\overline{S}_{33} = S_{33}$$

$$\overline{S}_{36} = 2(S_{13} - S_{23})\cos\theta\sin\theta + S_{36}(\cos^2\theta - \sin^2\theta)$$

$$\overline{S}_{44} = S_{44}\cos^2\theta + 2S_{45}\cos\theta\sin\theta + S_{55}\sin^2\theta$$

$$\overline{S}_{45} = S_{45}(\cos^2\theta - \sin^2\theta) + (S_{55} - S_{44})\cos\theta\sin\theta$$

$$\overline{S}_{55} = S_{55}\cos^2\theta + S_{44}\sin^2\theta - 2S_{45}\cos\theta\sin\theta$$

$$\overline{S}_{66} = S_{66}(\cos^2\theta - \sin^2\theta)^2 + 4(S_{16} - S_{26})(\cos^2\theta - \sin^2\theta)\cos\theta\sin\theta + 4(S_{11} + S_{22} - 2S_{12})\cos^2\theta\sin^2\theta \tag{2.8}$$

The stress-strain relations in x-y-z coordinates are,

$$\begin{Bmatrix} \sigma_x \\ \sigma_y \\ \sigma_z \\ \tau_{yz} \\ \tau_{xz} \\ \tau_{xy} \end{Bmatrix} = \begin{bmatrix} \overline{C}_{11} & \overline{C}_{12} & \overline{C}_{13} & 0 & 0 & \overline{C}_{16} \\ \overline{C}_{21} & \overline{C}_{22} & \overline{C}_{23} & 0 & 0 & \overline{C}_{26} \\ \overline{C}_{31} & \overline{C}_{32} & \overline{C}_{33} & 0 & 0 & \overline{C}_{36} \\ 0 & 0 & 0 & \overline{C}_{44} & \overline{C}_{45} & 0 \\ 0 & 0 & 0 & \overline{C}_{45} & \overline{C}_{55} & 0 \\ \overline{C}_{16} & \overline{C}_{26} & \overline{C}_{36} & 0 & 0 & \overline{C}_{66} \end{bmatrix} \begin{Bmatrix} \varepsilon_x \\ \varepsilon_y \\ \varepsilon_z \\ \gamma_{yz} \\ \gamma_{xz} \\ \gamma_{xy} \end{Bmatrix} \tag{2.9}$$

The transformed compliance coefficients $\overline{C}_{ij}$, referred to the (x, y, z) system,

$$\overline{C}_{11} = C_{11}\cos^4\theta - 4C_{16}\cos^3\theta\sin\theta + 2(C_{12} + C_{66})\cos^2\theta\sin^2\theta - 4C_{26}\cos\theta\sin^3\theta + C_{22}\sin^4\theta$$

$$\overline{C}_{12} = C_{12}\cos^4\theta + 2(C_{16} - C_{26})\cos^3\theta\sin\theta + (C_{11} + C_{12} - 4C_{66})\cos^2\theta\sin^2\theta + 2(C_{26} - C_{16})\cos\theta\sin^3\theta + C_{12}\sin^4\theta$$

$$\overline{C}_{13} = C_{13}\cos^2\theta - 2C_{36}\cos\theta\sin\theta + C_{23}\sin^2\theta$$

$$\overline{C}_{16} = C_{16}\cos^4\theta + (C_{11} - C_{12} - 2C_{66})\cos^3\theta\sin\theta + 3(C_{26} - C_{16})\cos^2\theta\sin^2\theta + (2C_{66} + C_{12} - C_{22})\cos\theta\sin^3\theta - C_{26}\sin^4\theta$$

$$\overline{C}_{22} = C_{22}\cos^4\theta + 4C_{26}\cos^3\theta\sin\theta + 2(C_{12} + 2C_{66})\cos^2\theta\sin^2\theta + 4C_{16}\cos\theta\sin^3\theta + C_{11}\sin^4\theta$$

$$\overline{C}_{23} = C_{23}\cos^2\theta + 2C_{36}\cos\theta\sin\theta + C_{13}\sin^2\theta$$

$$\overline{C}_{26} = C_{26}\cos^4\theta + (C_{12} - C_{22} + 2C_{66})\cos^3\theta\sin\theta + 3(C_{16} - C_{26})\cos^2\theta\sin^2\theta + (C_{11} - C_{12} - 2C_{66})\cos\theta\sin^3\theta - C_{16}\sin^4\theta$$

$$\overline{C}_{33} = C_{33}$$

$$\overline{C}_{36} = (C_{13} - C_{23})\cos\theta\sin\theta + C_{36}(\cos^2\theta - \sin^2\theta)$$

$$\overline{C}_{44} = C_{44}\cos^2\theta + C_{55}\sin^2\theta + 2C_{45}\cos\theta\sin\theta$$

$$\overline{C}_{45} = C_{45}(\cos^2\theta - \sin^2\theta) + (C_{55} - C_{44})\cos\theta\sin\theta$$

$$\overline{C}_{55} = C_{55}\cos^2\theta + C_{44}\sin^2\theta - 2C_{45}\cos\theta\sin\theta$$

$$\overline{C}_{66} = 2(C_{16} - C_{26})\cos^3\theta\sin\theta + (C_{11} + C_{22} - 2C_{12} - 2C_{66})\cos^2\theta\sin^2\theta + 2(C_{26} - C_{16})\cos\theta\sin^3\theta + C_{66}(\cos^4\theta + \sin^4\theta) \tag{2.10}$$

Note that C_{14}, C_{15}, C_{16}, C_{24}, C_{25}, C_{26}, C_{34}, C_{35}, C_{36}, C_{45}, C_{46}, and C_{56} are zero for an orthotropic material.

2.1.3 Classical Lamination Theory

A laminate is two or more lamina bonded together to act as an integral structural element. A typical laminate is shown in Figure 3.4. Laminated composite materials typically have exceptional properties in the direction of the reinforcing fibers, but poor to mediocre properties perpendicular (transverse) to the fibers. The problem is how to obtain maximum advantage from the exceptional fiber directional properties while minimizing the effects of the low transverse properties. The plies or lamina principal material directions are oriented in several directions such that the effective properties of the laminate match the loading environment. For purposes of structural analysis, it is desirable to represent a laminate by set of effective stiffness. The stiffness of such a composite material configuration is obtained from the properties of the constituent lamina. The procedures enable the analysis of laminates that have individual lamina with principal material directions oriented at arbitrary angles to the chosen or natural axes of the laminate. As a consequence of the arbitrary orientations, the laminate may not have definable principal directions.

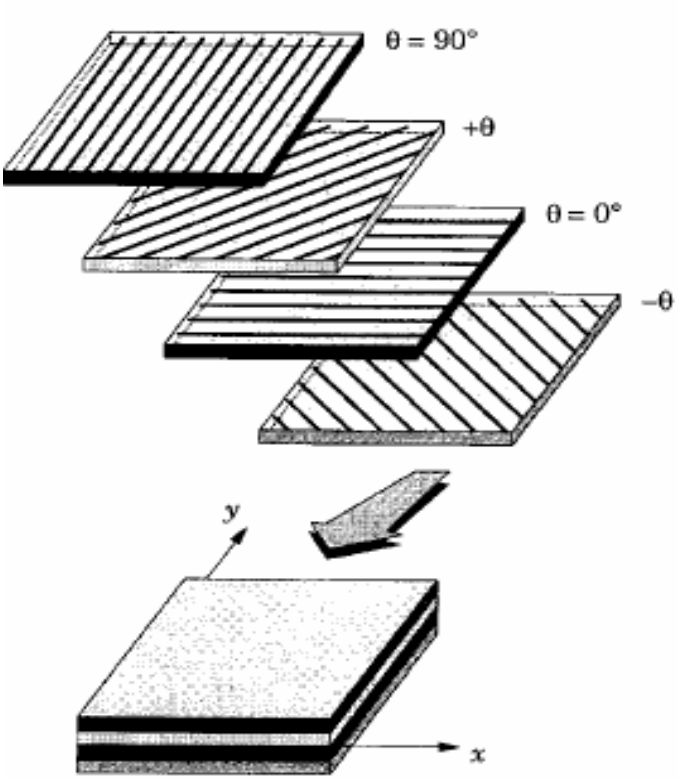

Figure 2.3 A laminate made up of lamina with different fiber orientations

It is apparent that overall behavior of a multidirectional laminate is a function of the properties and stacking sequence of the individual layers. The so-called classical lamination theory predicts the behavior of the laminate within the framework. By use of this theory, it can be consistently proceed from the basic building block, the lamina, to the end result, a structural laminate.

2.1.4 Strain and Stress Variation in a Laminate

Knowledge of the variation of stress and strain through the laminate thickness is essential to the definition of the extensional and bending stiffness of a laminate. In the classical lamination theory, the laminate is presumed to consist of perfectly bonded lamina. Moreover, the bonds are presumed to be infinitesimally thin as well as non-shear deformable. That is, the displacements are continuous across lamina boundaries so that no lamina can slip relative to another. Thus, the laminate acts as a single with very special properties, but nevertheless acts as a single layer of material.

Accordingly, if the laminate is thin, a line originally straight and perpendicular to the middle surface of the laminate is assumed to remain straight and perpendicular to the middle surface when the laminate is extended and bent. Requiring the normal to the middle surface to remain straight and normal under deformation is equivalent to ignoring the shearing strains in planes perpendicular to the middle surface, that is $\gamma_{xz}=\gamma_{yz}= 0$ where z is the direction of the normal to the middle surface in Figure 2.4. In addition, the normals are presumed to have constant length so that the strain perpendicular to the middle surface is ignored as well, that is, $\varepsilon_z=0$. The foregoing collection of assumptions of the behavior of the single layer that represents the laminate constitutes the familiar Kirchhoff hypothesis for plates and the Kirchhoff-Love hypothesis for shells.

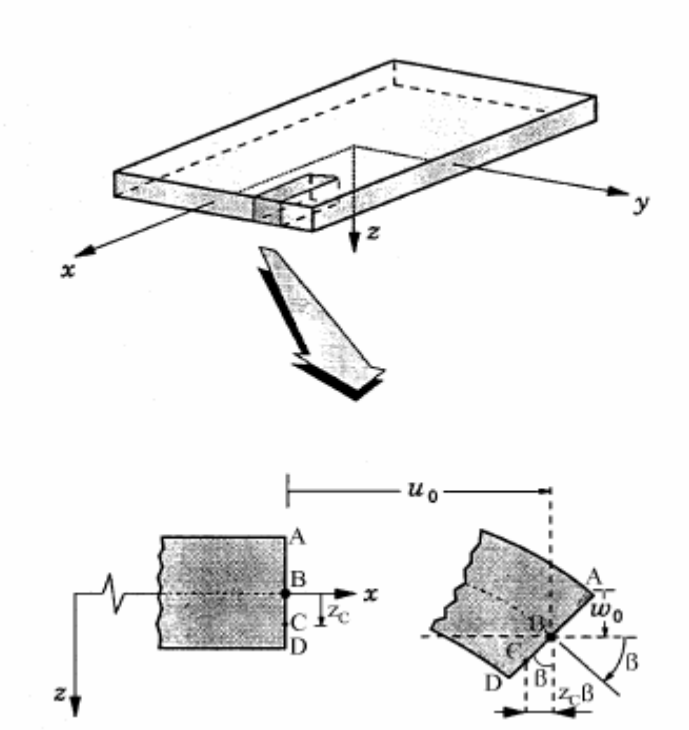

Figure 2.4 Undeformed and deformed geometries of
an edge of a plate under the Kirchoff assumptions

The implications of the Kirchhoff or the Kirchhoff-Love hypothesis on the laminate displacements u, v, and w in the x, y, and z directions are derived by use of the laminate cross section in the x-z plane shown in Figure 2.4. The displacement in the x-direction of point B from the un-deformed to the deformed middle surface is u_0. Since line ABCD remains straight under deformation of the laminate, the displacement that

$$u_c=u_0-z_c\beta \tag{2.11}$$

But since, under deformation, line ABCD further remains perpendicular to the middle surface, β is the slope of the laminate middle surface in the x-direction, that is,

$$\beta = \frac{\partial w_0}{\partial x} \tag{2.12}$$

Then, the displacement, u, at any point z through the laminate thickness is

$$u = u_0 - z\frac{\partial w_0}{\partial x} \tag{2.13}$$

By similar reasoning, the displacement, v, in the y-direction is

$$v = v_0 - z\frac{\partial w_0}{\partial y} \tag{2.14}$$

The laminate strains have been reduced to ε_x, ε_y, γ_{xy} virtue of the Kirchhoff-Love hypothesis. That is, $\varepsilon_z = \gamma_{xz} = \gamma_{yz} = 0$. For small strains (linear elasticity), the remaining strains are defined in terms of displacements as

$$\varepsilon_x = \frac{\partial u}{\partial x}$$

$$\varepsilon_y = \frac{\partial v}{\partial y} \tag{2.15}$$

$$\gamma_{xy} = \frac{\partial u}{\partial y} + \frac{\partial v}{\partial x}$$

Thus, for the derived displacements u and v Eq. (2.13) and (2.14) and the strains are

$$\varepsilon_x = \frac{\partial u_0}{\partial x} - z\frac{\partial^2 w_0}{\partial x^2}$$

$$\varepsilon_y = \frac{\partial v}{\partial y} - z\frac{\partial^2 w_0}{\partial y^2} \tag{2.16}$$

$$\gamma_{xy} = \frac{\partial u_0}{\partial y} + \frac{\partial v_0}{\partial x} - 2z\frac{\partial^2 w_0}{\partial x \partial y}$$

or

$$\begin{Bmatrix} \varepsilon_x \\ \varepsilon_y \\ \gamma_{xy} \end{Bmatrix} = \begin{Bmatrix} \varepsilon_x^0 \\ \varepsilon_y^0 \\ \gamma_{xy}^0 \end{Bmatrix} + z\begin{Bmatrix} K_x \\ K_y \\ K_{xy} \end{Bmatrix} \tag{2.17}$$

where the middle surface strains are

$$\begin{Bmatrix} \varepsilon_x^0 \\ \varepsilon_y^0 \\ \gamma_{xy}^0 \end{Bmatrix} = \begin{Bmatrix} \dfrac{\partial u_0}{\partial x} \\ \dfrac{\partial v_0}{\partial y} \\ \dfrac{\partial u_0}{\partial y} + \dfrac{\partial v_0}{\partial x} \end{Bmatrix} \tag{2.18}$$

and the middle surface curvatures are

$$\begin{Bmatrix} K_x \\ K_y \\ K_{xy} \end{Bmatrix} = -\begin{Bmatrix} \dfrac{\partial^2 w_0}{\partial x^2} \\ \dfrac{\partial^2 w_0}{\partial y^2} \\ 2\dfrac{\partial^2 w_0}{\partial x \partial y} \end{Bmatrix} \tag{2.19}$$

The last term in Eq. (2.19) is the twist curvature of the middle surface.

By substitution of the strain variation through the thickness, Eq. (2.17), in the stress strain relations, Eq. (2.9), the stresses in the kth layer can be expressed in terms of the laminate middle surface strains and curvatures as

$$\begin{Bmatrix} \sigma_x \\ \sigma_y \\ \tau_{xy} \end{Bmatrix}_k = \begin{bmatrix} \overline{Q}_{11} & \overline{Q}_{12} & \overline{Q}_{16} \\ \overline{Q}_{12} & \overline{Q}_{22} & \overline{Q}_{26} \\ \overline{Q}_{16} & \overline{Q}_{26} & \overline{Q}_{66} \end{bmatrix}_k \left\{ \begin{Bmatrix} \varepsilon_x^0 \\ \varepsilon_y^0 \\ \gamma_{xy}^0 \end{Bmatrix} + z \begin{Bmatrix} K_x \\ K_y \\ K_{xy} \end{Bmatrix} \right\} \tag{2.20}$$

Since the $\overline{Q}_{ij}$ can be different for each layer of the laminate, the stress variation through the laminate thickness is not necessarily linear, even though the strain variation is linear.

2.1.5 Resultant Laminate Forces and Moments

The resultant forces and moments acting on a laminate are obtained by integration of the stresses in each layer or lamina through the laminate thickness, for example

$$N_x = \int_{-t/2}^{t/2} \sigma_x dz$$
$$M_x = \int_{-t/2}^{t/2} \sigma_x z dz \qquad (2.21)$$

N_x is a force per unit length (width) of the cross section of the laminate. Similarly, M_x is a moment per unit length as shown Figure 2.5. The entire collection of force and moment resultants for an N-layered laminate is defined as

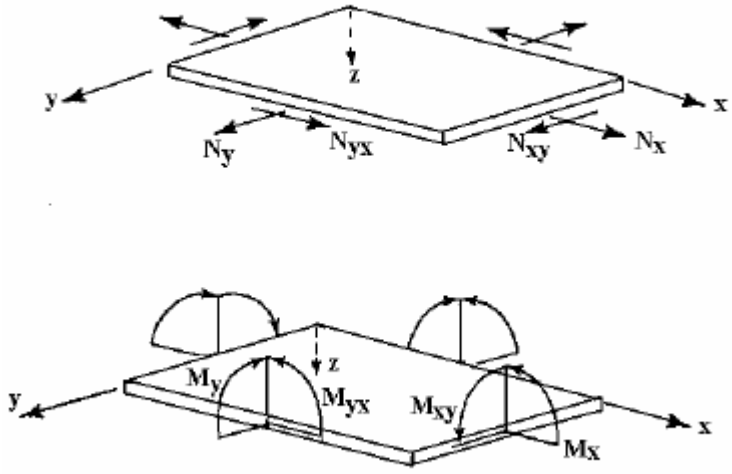

Figure 2.5 In-plane forces and moments on flat laminate

$$\begin{Bmatrix} N_x \\ N_y \\ N_{xy} \end{Bmatrix} = \int_{-t/2}^{t/2} \begin{Bmatrix} \sigma_x \\ \sigma_y \\ \tau_{xy} \end{Bmatrix}_k dz = \sum_{k=1}^{N} \int_{z_{k-1}}^{z_k} \begin{Bmatrix} \sigma_x \\ \sigma_y \\ \tau_{xy} \end{Bmatrix}_k dz \qquad (2.22)$$

$$\begin{Bmatrix} M_x \\ M_y \\ M_{xy} \end{Bmatrix} = \int_{-t/2}^{t/2} \begin{Bmatrix} \sigma_x \\ \sigma_y \\ \tau_{xy} \end{Bmatrix}_k z dz = \sum_{k=1}^{N} \int_{z_{k-1}}^{z_k} \begin{Bmatrix} \sigma_x \\ \sigma_y \\ \tau_{xy} \end{Bmatrix}_k z dz \qquad (2.23)$$

where z_k and z_{k-1} are defined in Figure 2.6. These force and moment resultants do not depend on z after integration, but are functions of x and y, the coordinates in the plane of the laminate middle surface.

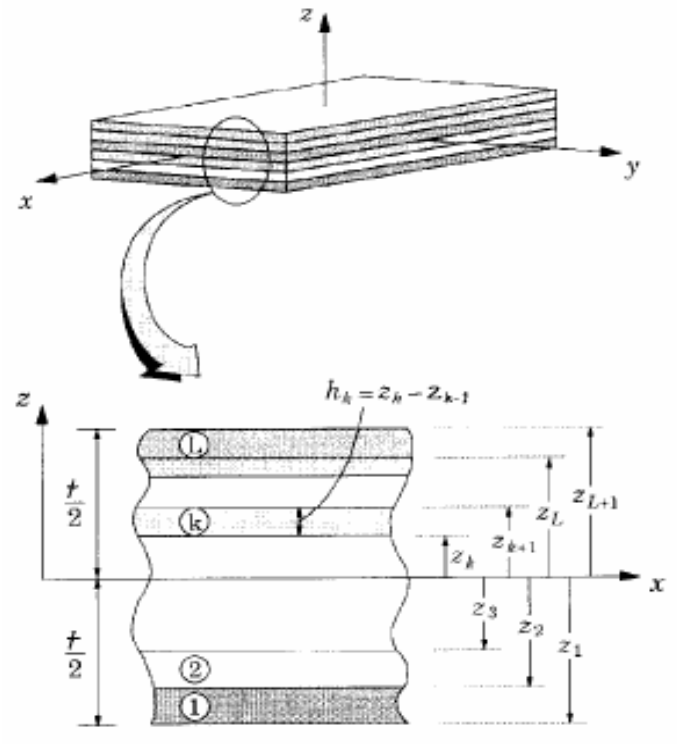

Figure 2.6 Geometry of an N-layered laminate

The integration indicated in Eq. (2.22) and (2.23) can be rearranged to take advantage of the fact that the stiffness matrix for a lamina is constant within the lamina. Thus, the stiffness matrix goes outside the integration over each layer. When the Eq. (2.20) are substituted, the forces and moments become

$$\begin{Bmatrix} N_x \\ N_y \\ N_{xy} \end{Bmatrix} = \sum_{k=1}^{N} \begin{bmatrix} \overline{Q}_{11} & \overline{Q}_{12} & \overline{Q}_{16} \\ \overline{Q}_{12} & \overline{Q}_{22} & \overline{Q}_{26} \\ \overline{Q}_{16} & \overline{Q}_{26} & \overline{Q}_{66} \end{bmatrix}_k \left\{ \int_{z_{k-1}}^{z_k} \begin{Bmatrix} \varepsilon_x^0 \\ \varepsilon_y^0 \\ \gamma_{xy}^0 \end{Bmatrix} dz + \int_{z_{k-1}}^{z_k} \begin{Bmatrix} K_x \\ K_y \\ K_{xy} \end{Bmatrix} z dz \right\} \tag{2.24}$$

$$\begin{Bmatrix} M_x \\ M_y \\ M_{xy} \end{Bmatrix} = \sum_{k=1}^{N} \begin{bmatrix} \overline{Q}_{11} & \overline{Q}_{12} & \overline{Q}_{16} \\ \overline{Q}_{12} & \overline{Q}_{22} & \overline{Q}_{26} \\ \overline{Q}_{16} & \overline{Q}_{26} & \overline{Q}_{66} \end{bmatrix}_k \left\{ \int_{z_{k-1}}^{z_k} \begin{Bmatrix} \varepsilon_x^0 \\ \varepsilon_y^0 \\ \gamma_{xy}^0 \end{Bmatrix} z dz + \int_{z_{k-1}}^{z_k} \begin{Bmatrix} K_x \\ K_y \\ K_{xy} \end{Bmatrix} z^2 dz \right\} \tag{2.25}$$

However, ε_x^0, ε_y^0, γ_{xy}, K_x, K_y and K_{xy} are not functions of z but are middle surface values so can be removed from under the summation signs. Thus,

$$\begin{Bmatrix} N_x \\ N_y \\ N_{xy} \end{Bmatrix} = \begin{bmatrix} A_{11} & A_{12} & A_{16} \\ A_{12} & A_{22} & A_{26} \\ A_{16} & A_{26} & A_{66} \end{bmatrix} \begin{Bmatrix} \varepsilon_x{}^0 \\ \varepsilon_y{}^0 \\ \varepsilon_{xy}{}^0 \end{Bmatrix} + \begin{bmatrix} B_{11} & B_{12} & B_{16} \\ B_{12} & B_{22} & B_{26} \\ B_{16} & B_{26} & B_{66} \end{bmatrix} \begin{Bmatrix} K_x \\ K_y \\ K_{xy} \end{Bmatrix}$$

$$\begin{Bmatrix} M_x \\ M_y \\ M_{xy} \end{Bmatrix} = \begin{bmatrix} B_{11} & B_{12} & B_{16} \\ B_{12} & B_{22} & B_{26} \\ B_{16} & B_{26} & B_{66} \end{bmatrix} \begin{Bmatrix} \varepsilon_x{}^0 \\ \varepsilon_y{}^0 \\ \varepsilon_{xy}{}^0 \end{Bmatrix} + \begin{bmatrix} D_{11} & D_{12} & D_{16} \\ D_{12} & D_{22} & D_{26} \\ D_{16} & D_{26} & D_{66} \end{bmatrix} \begin{Bmatrix} K_x \\ K_y \\ K_{xy} \end{Bmatrix} \tag{2.26}$$

where

$$\begin{aligned} A_{ij} &= \sum_{k=1}^{N} \left(\overline{Q}_{ij}\right)_k \left(z_k - z_{k-1}\right) \\ B_{ij} &= \frac{1}{2} \sum_{k=1}^{N} \left(\overline{Q}_{ij}\right)_k \left(z^2{}_k - z^2{}_{k-1}\right) \\ D_{ij} &= \frac{1}{3} \sum_{k=1}^{N} \left(\overline{Q}_{ij}\right)_k \left(z^3{}_k - z^3{}_{k-1}\right) \end{aligned} \tag{2.27}$$

The complete set of the equations can be expressed in matrix form as

$$\begin{Bmatrix} N_x \\ N_y \\ N_{xy} \\ M_x \\ M_y \\ M_{xy} \end{Bmatrix} = \begin{bmatrix} A_{11} & A_{12} & A_{16} & B_{11} & B_{12} & B_{16} \\ A_{12} & A_{22} & A_{26} & B_{12} & B_{22} & B_{26} \\ A_{16} & A_{26} & A_{66} & B_{16} & B_{26} & B_{66} \\ B_{11} & B_{12} & B_{16} & D_{11} & D_{12} & D_{16} \\ B_{12} & B_{22} & B_{26} & D_{12} & D_{22} & D_{26} \\ B_{16} & B_{26} & B_{66} & D_{16} & D_{26} & D_{66} \end{bmatrix} \begin{Bmatrix} \varepsilon_x{}^0 \\ \varepsilon_y{}^0 \\ \varepsilon_{xy}{}^0 \\ K_x \\ K_y \\ K_{xy} \end{Bmatrix} \tag{2.28}$$

Or in partitioned form as

$$\begin{Bmatrix} N \\ M \end{Bmatrix} = \begin{bmatrix} A & B \\ B & D \end{bmatrix} \begin{Bmatrix} \varepsilon^0 \\ K \end{Bmatrix} \tag{2.29}$$

Since the applied loads are generally known rather than the deformations, it is often necessary to use the inverted form of the laminate force-deformation relationships.

$$\begin{Bmatrix} \varepsilon^0 \\ K \end{Bmatrix} = \begin{bmatrix} A & B \\ B & D \end{bmatrix}^{-1} \begin{Bmatrix} N \\ M \end{Bmatrix} \tag{2.30}$$

The relations above are expressed in terms of three laminate stiffness matrices. [A], [B] and [D], which are functions of the geometry, material properties and stacking sequence of the individual plies, as described in Eq. (2.27). They are average elastic parameters of the multidirectional laminate with the following significance:

A_{ij} are extensional stiffnesses, or in-plane laminate moduli, relating in-plane loads toin-plane strains. Bij are called coupling stiffness, or in-plane flexure coupling laminatemoduli, relating in-plane loads to curvatures and moments to in-plane strains. Thus, if $B_{ij}\neq 0$, in-plane forces produce flexural and twisting deformations; moments produceextension of the middle surface in addition to flexure and twisting. D_{ij} are bending or flexural laminate stiffnesses relating moments to curvatures.

2.1.6 Symmetric Laminates

A laminate is called symmetric when for each layer on one side of a reference plane(middle surface) there is a corresponding layer at an equal distance from the referenceplane on the other side with identical thickness, orientation, and properties. The laminateis symmetric in both geometry and material properties.

Consider the N-layer laminate in Figure 2.7, where identical layers k and k′ aresymmetrically situated about the reference plane. Then

$$\begin{aligned} t_k &= t_k' \\ \left(\overline{Q}_{ij}\right)_k &= \left(\overline{Q}_{ij}\right)_{k'} \\ h_k &= -h_k' \end{aligned} \tag{2.31}$$

and according to the definition in Eq. (2.27), the coupling stiffness are

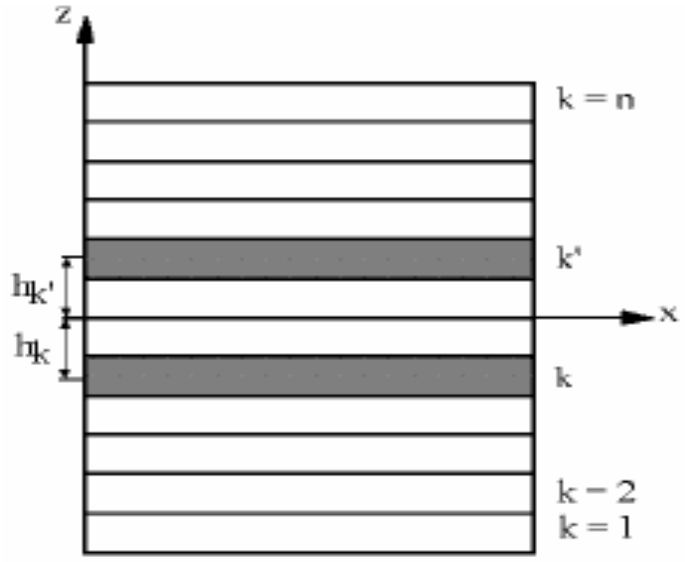

Figure 2.7 Symmetric laminate with identical layers k and k′

$$B_{ij} = \frac{1}{2}\sum_{k=1}^{N}\left(\overline{Q}_{ij}\right)_k \left(z^2{}_k - z^2{}_{k-1}\right)$$

$$B_{ij} = \frac{1}{2}\sum_{k=1}^{N}\left(\overline{Q}_{ij}\right)_k \left(z_k + z_{k-1}\right)\left(z_k - z_{k-1}\right) \qquad (2.32)$$

$$B_{ij} = \sum_{k=1}^{N}\left(\overline{Q}_{ij}\right)_k h_k .t_k$$

Since

$$h_k = \frac{1}{2}\left(z_k + z_{k-1}\right)$$

$$t_k = z_k - z_{k-1} \qquad (2.33)$$

For the conditions of symmetry stated before, the sum above will consist of pairs ofterms of equal absolute value and opposite signs. Thus, such a symmetry condition whensubstituted in Eq. (2.27) leads to the major simplification that all $B_{ij} = 0$. This means that bending-stretching coupling will not be present in such laminates. Consequently, inplane loads will not generate bending and twisting curvatures that

cause out-of-plane warping, and bending or twisting moments will not produce on extension of the middle surface.

The load-deformation relations in this case reduce to

$$\begin{Bmatrix} N_x \\ N_y \\ N_{xy} \end{Bmatrix} = \begin{bmatrix} A_{11} & A_{12} & A_{16} \\ A_{12} & A_{22} & A_{26} \\ A_{16} & A_{26} & A_{66} \end{bmatrix} \begin{Bmatrix} \varepsilon_x^{\,0} \\ \varepsilon_y^{\,0} \\ \gamma_{xy}^{\,0} \end{Bmatrix}$$

$$\begin{Bmatrix} M_x \\ M_y \\ M_{xy} \end{Bmatrix} = \begin{bmatrix} D_{11} & D_{12} & D_{16} \\ D_{12} & D_{22} & D_{26} \\ D_{16} & D_{26} & D_{66} \end{bmatrix} \begin{Bmatrix} K_x \\ K_y \\ K_{xy} \end{Bmatrix} \tag{2.34}$$

2.2 Failure Analysis

To analyze the strength of any laminated composite, strength theories are required. Failure analysis is a tool for predicting the strength of a laminated composite, containing several plies with different orientations, under complex loading conditions using strength data obtained from uniaxial tests of unidirectional plies and strength theories. There are numerous failure criteria for composite materials as a direct result of the complex nature of observed failure phenomena. These criteria are only useful if they can be incorporated into a progressive damage analysis, which usually means that they must be compatible with a finite element formulation.

Different types of failure criteria have been used for failure design of composite laminates. In general, the failure criteria are categorized into two: independent and interactive (or quadratic polynomial) criteria. An independent criterion, such as maximum stress or maximum strain, is simple to apply and more significantly, tells the mode of failure, but it neglects the effect of stress interactions. For this reason, these criteria are quite conservative. An interactive criterion, such as Tsai-Wu, Tsai-Hill, Hoffmann includes stress interactions in the failure mechanism and predicts first ply failure but it requires some efforts to determine parameters.

Hashin failure criteria (1980) are polynominal failure criteria similar to the quadratic failure envelope except that in the Hashin formulation there are distinct polynomials corresponding to the different modes. Hashin-type failure criteria are ideal for use in finite element models, especially when adapted to progressive damage models. Hashin proposed a set of failure criteria for predicting failure of unidirectional composites based on each failure mode (Lessard & Shokrieh, 1995).

2.2.1 Hashin Failure Criterion 3D

Matrix Tensile Failure

$$\frac{1}{Y_T^2}(\sigma_2+\sigma_3)^2+\frac{1}{S_T^2}\left(\tau_{23}^2-\sigma_2\sigma_3\right)+\frac{1}{S^2}\left(\tau_{12}^2+\tau_{13}^2\right)=1 \tag{2.35}$$

where σ_2 and σ_3 are the normal stresses in the transverse directions to fibers of the lamina. $\tau_{23,}$ τ_{13} and τ_{12} are the shear stresses in the lamina.

Y_T is the tensile strength in the transverse direction of the fibers.
S is the shear strength, in the 1-2 plane of the lamina.
S_T is the transverse shear strength in the 1-3 and 2-3 planes of the lamina.

Matrix Compression Failure

$$\frac{1}{Y_C}\left[\left(\frac{Y_C}{2S_T}\right)^2-1\right](\sigma_2+\sigma_3)+\frac{1}{4S_T{}^2}(\sigma_2+\sigma_3)^2+\frac{1}{S_T^2}\left(\tau_{23}^2-\sigma_2\sigma_3\right)$$
$$+\frac{1}{S^2}\left(\tau_{12}^2+\tau_{13}^2\right)=1 \tag{2.36}$$

where Y_C is the compression strength in the transverse direction of the fibers.

Fiber Tensile Failure

$$\left(\frac{\sigma_1}{X_T}\right)^2 + \frac{1}{S^2}\left(\tau_{12}^2 + \tau_{13}^2\right) = 1 \tag{2.37}$$

where σ_1 is the normal stress in the direction of the fibers of the lamina and X_T is the tensile strength of the fibers.

Fiber Compression Failure

$$\left|\sigma_1\right| = X_C \tag{2.38}$$

where X_C is the compressive strength of the fibers.

CHAPTER THREE
EXPERIMENTAL STUDY

3.1 Problem Statement

In this study, composite rectangular plate (length L, width W, thickness t) made of N fiber-reinforced unidirectional plies with two circular holes filled with two rigid pin is used. The holes diameter (D) were fixed at a constant value of 5 mm. The first hole is located along the centerline of the plate at a distance E from end of the plate. The second hole is located at a distance K from the first hole. The geometry of problem is shown in Figure 3.1. A uniform tensile load P is applied to the plate. Load is parallel to the plate and is symmetric with respect to the centreline. Thus, the load can not create bending moments about x, y, z-axes.

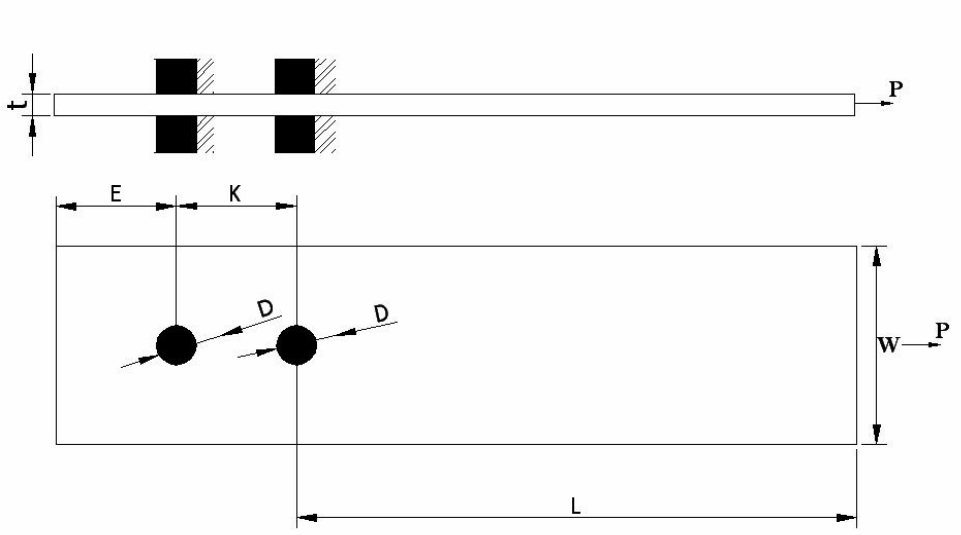

D = 5 mm

t = 2.8 mm

Figure 3.1 Geometry of a laminated composite plate with two circular holes

In the plate of arbitrary orientation, the ratio of width to diameter, W/D, ratio was 2, 3, 4, 5. The edge distance to diameter, E/D, ratio was 1, 2, 3, 4, 5. Furthermore, the distance between two holes to diameter, K/D, ratio was 2, 3, 4, 5. To estimate the

strength of the specimens with two pin loaded in series, the static bearing strength is defined as:

$$\sigma_b = \frac{P}{D.t} \tag{3.1}$$

The joints is maimly governed by the shear and the tensile strengths of the pins, composite joints present specific failure modes due to their heterogeneity and anisotropy. Three main basic failure modes are often described in the literature : bearing, net-tension and shear-out.

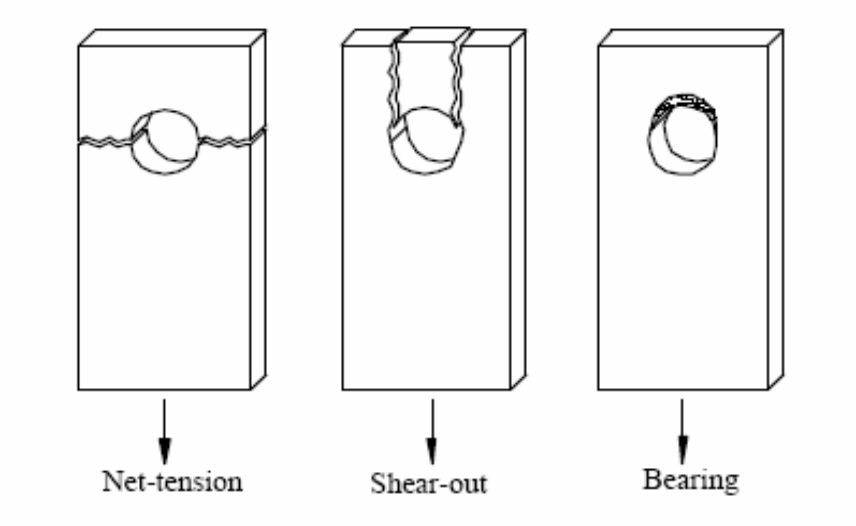

Figure 3.2. Typical failure mechanisms for the pinned-joint configuration

The behavior of joint could be influenced by four groups of parameters (Chen et al., 1994).

- Material parameters : fiber types and form, resin type, fiber orientation, laminate stacking sepuence, etc.
- Geometry parameters : specimen width (W) or ratio of width to hole diameter (W/D), edge distance (E) or ratio of the edge distance to hole diameter (E/D), specimen thickness (t), hole size (D) and pitch for multiple joints.

- Fastener parameters : fastener type, fastener size, clamping area and pressure, washer size and hole size and tolerance.

- Design parameters : loading type (tension, compression, fatigue, etc.), loading direction, joint type (single lap, double lap), geometry (pitch, edge distance, hole pattern etc.), environment and failure criteria.

3.2 Manufacturing of the Specimens

The glass-vinylester composite specimens used in this study were produced at IZOREEL firm. The woven glass-vinylester prepregs are cured about 30 minutes at 100 °C under 10 MPa pressure. Composite plate was consisted of twelve laminas. Thickness of each lamina was 0.3 mm. These laminas were stuck on each other by hydraulic press. At the end of the manufacturing, composite plate thickness was measured as 2.8 mm. Volume fraction of the glass fiber was approximately 63 %.

3.3 Determination of Mechanical Properties

To obtain $E_{1,}$ ν_{12} and $X_{t,}$ a regtangular specimen whose fiber direction coincidies with the loading direction on (Figure 3.3) is prepared and two strain gauges perpendicular to each other are stuck on (Figure 3.4). One of them is in the fiber direction the other in the transverse direction.

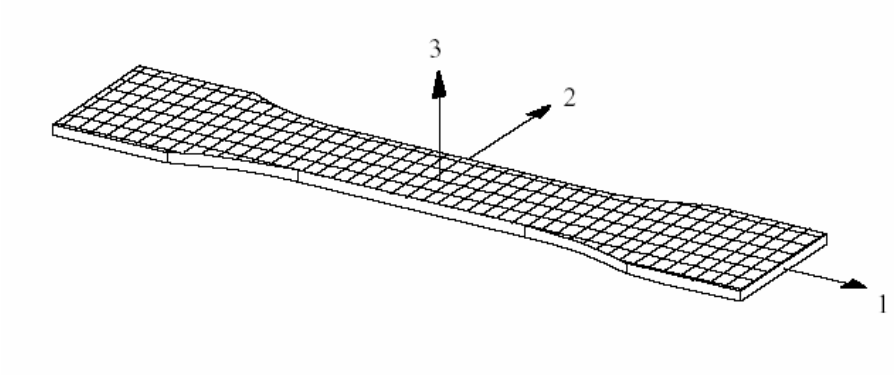

Figure 3.3 Direction of fibers on tensile specimen

The specimen is loaded step by step to rapture by Shimadzu Tensile Machine. For all steps, ε_1 and ε_2 are measured by an indicator. By using these strains $E_{1,}$ and ν_{12} are obtained. E_2 is assumed to be equal to E_1 because of the woven structure.

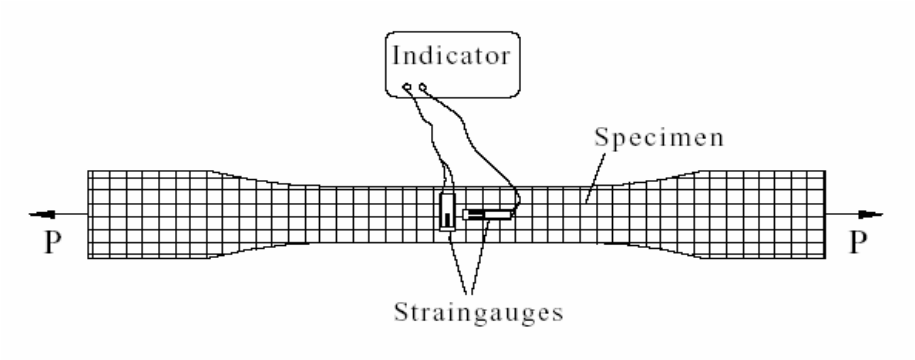

Figure 3.4 Longitudinal tension test specimen for determination of E_1, and ν_{12}

$$\sigma_1 = \frac{P}{A}, \qquad E_1 = \frac{\sigma_1}{\varepsilon_1}, \qquad E_2 = E_1, \qquad \nu_{12} = -\frac{\varepsilon_2}{\varepsilon_1} \tag{3.2}$$

X_t is calculated by dividing the ultimate force by the cross-sectional area of the specimen.

$$X_t = \frac{P_{ult}}{A} \tag{3.3}$$

To find X_c, a rectangular specimen with small length whose fiber direction coincides with the loading direction is taken and it is subjected to compressive loading (Figure 3.5). X_c is also calculated by dividing the ultimate force by the cross-sectional area of the specimen.

$$X_c = \frac{P_{ult}}{A} \tag{3.4}$$

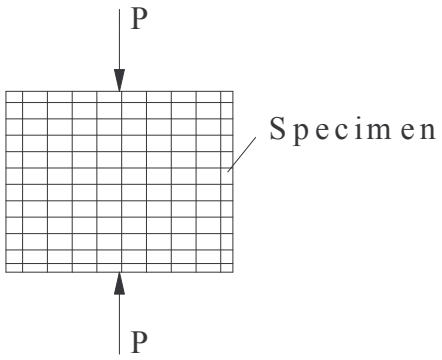

Figure 3.5 Compression test

To define the shear modulus G_{12}, a specimen whose principal axis is on 45° is taken and a strain gauge is stuck on loading direction of the lamina (Figure 3.6). The specimen is loaded step by step up to rapture by the test machine and G_{12} is calculated by measurement of the strain in the tensile direction, ε_x.

$$E_x = \frac{P/A}{\varepsilon_x}$$

$$G_{12} = \frac{1}{\frac{4}{E_x} - \frac{1}{E_1} - \frac{1}{E_2} + \frac{2\nu_{12}}{E_1}} \tag{3.5}$$

The strain gauge can't be stuck to direction 3 because of the small thickness G_{13} and G_{23} isn't found by experiment. Therefore, it is assumed that, G_{13} and G_{23} are equal to G_{12}.

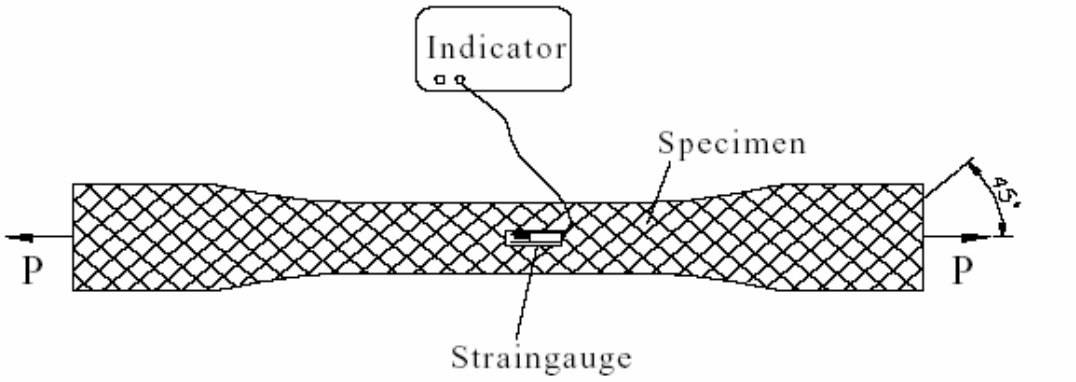

Figure 3.6 Off-axis test

Iosipescu testing method is used to define the shear strength S (Figure 3.7). The dimensions of the specimen are chosen as; a=80 mm, b=20 mm, c=12 mm and t_i=2,8 mm. A compression load is applied to the specimen. In failure, S is calculated from

$$S = \frac{P_{max}}{t_i . c} \tag{3.6}$$

where P_{max} is the failure force. (Okutan, 2001)

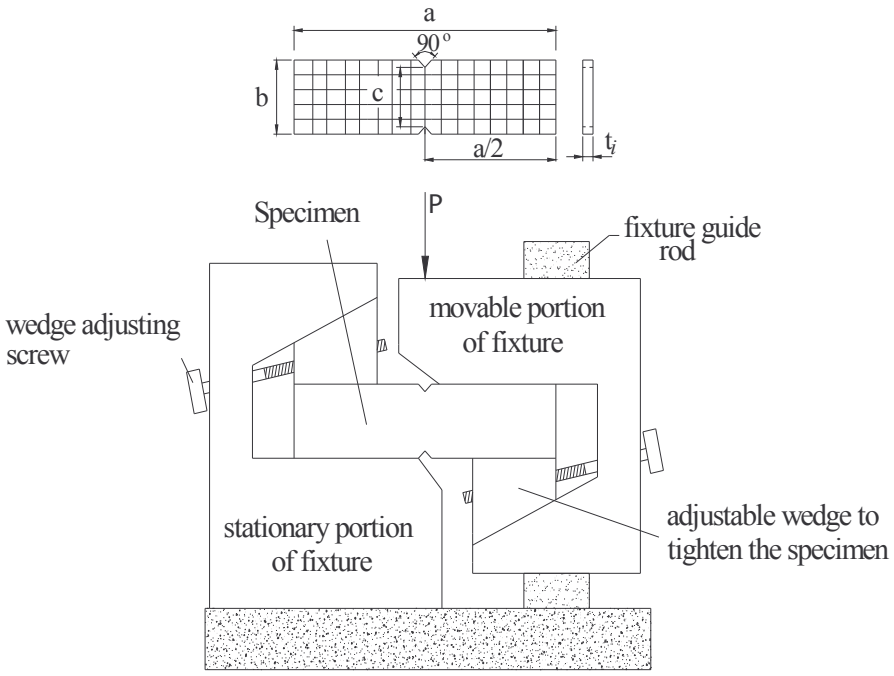

Figure 3.7 Iosipescu testing fixture

Y_t and Y_c are equal to, X_t and X_c, respectively because of the woven structure. The mechanical properties of glass-vinylester composite plate which are obtained from the experimental study have been given in Table 3.1. (Gülem, 2004)

Table 3.1 Mechanical properties of glass-vinlyester composite materials

$E_1=E_2$ (GPa)	G_{12} (GPa)	ν_{12}	$X_t=Y_t$ (MPa)	$X_c=Y_c$ (MPa)	S (MPa)	V_f (%)
20.769	4.133	0.09	395	260	75	63

3.4 Testing Procedures

To find the failure load and the failure mode, a series of experiments were performed. The specimens were trimmed as depicted in Figure 3.1. The effects of the pin location were studied by varying the width to diameter (W/D) ratio from 1 to 5, edge distance to diameter (E/D) ratio from 2 to 5 and between two holes distance to diameter (K/D) ratio from 2 to 5, for the 0° fiber orientation angle while keeping D, t

and L constant. 80 different geometries were used. All specimens were tested three times each.

The experiments were carried out in tension mode on the Tensile Machine. The lower edge of the specimen clamped and loaded from the steel pin by stretching the specimens at a ratio 0.5 mm/min Figure 3.8. The load-pin displacement diagrams for all composite configurations were plotted.

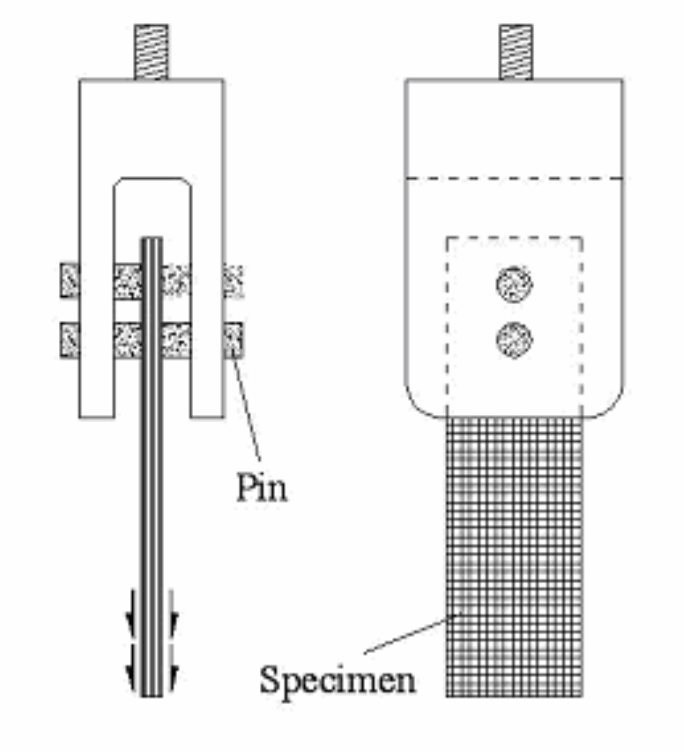

Figure 3.8 Experimental setup for pin-joint testing

CHAPTER FOUR
NUMERICAL STUDY

4.1 Introduction

In this chapter, by using LUSAS 13.3 finite element analysis program, a static progressive failure analysis was performed on eighty different pin-loaded composite plates. In addition, parametric studies have been performed using various geometry. The effects of material non-linearity on the prediction of the failure initiation and failure loads were studied.

4.2 Three-Dimensional Finite Element Method

In the three-dimensional finite element formulation, the displacements, traction components, and distributed body force values are the functions of the position indicated by (*x, y, z).* The displacement vector **u** is given as

$$\mathbf{u} = [u, v, w]^T \tag{4.1}$$

where *u,* ν and w are the *x, y* and *z* components of **u**, respectively. The stress and strains are given by

$$\sigma = [\sigma_{xx}, \sigma_{yy}, \sigma_{zz}, \sigma_{yz}, \sigma_{xz}, \sigma_{xy}]^T$$
$$\varepsilon = [\varepsilon_{xx}, \varepsilon_{yy}, \varepsilon_{zz}, \gamma_{yz}, \gamma_{xz}, \gamma_{xy}]^T \tag{4.2}$$

From Figure 4.1, representing the three- dimensional problem in a general setting, the body force and traction vector are given by

$$\mathbf{f} = [f_x, f_y, f_z]^T \quad , \ \mathbf{T} = [T_x, T_y, T_z]^T \tag{4.3}$$

The body force **f** has dimensions of force per unit volume, while the traction force **T** has dimensions of force per unit area.

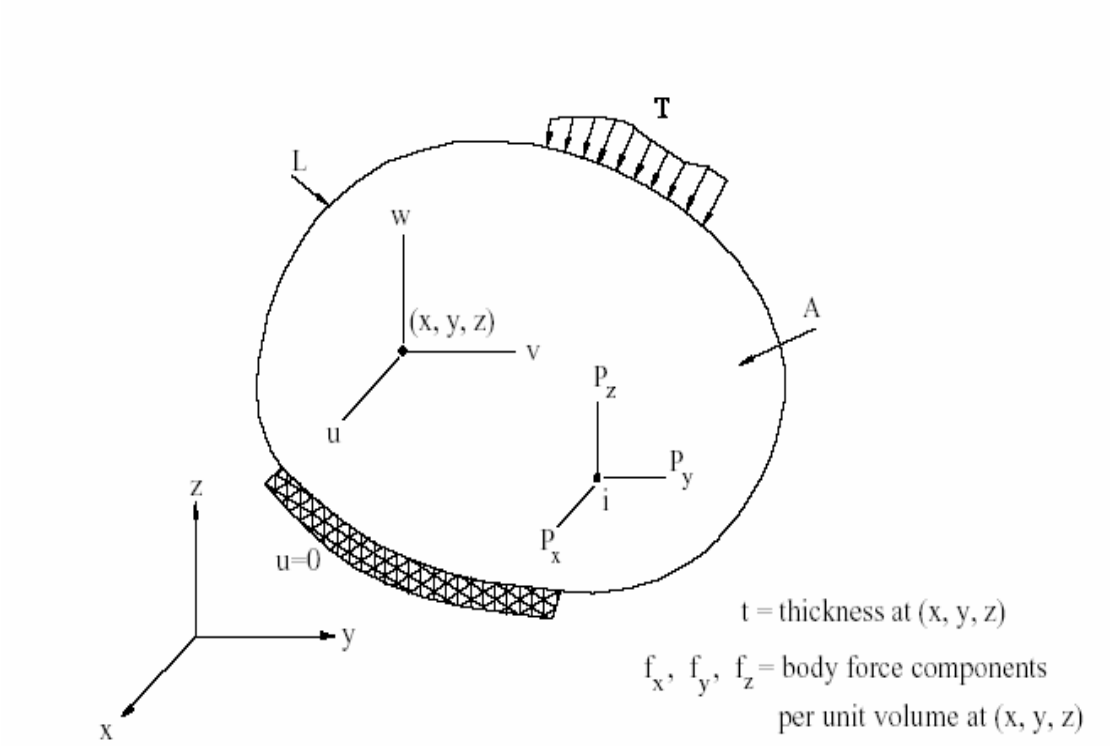

Figure 4.1 Three-dimensional problem

4.3 Modeling of the Problem

In this study, maximum failure load value was found by nonlinear analysis, after that failure strength properties carried out on the specimen. This example case of W/D=4, E/D=4, K/D=4 and θ =0° are chosen. In this example the composite plate will be modeled as a half model and symmetry boundary conditions are used to reduce the size of the model. In this example the mesh will be graded manually by specifying the number of elements on each of the boundary lines. The surface will now be swept through the depth of the plate to create a volume. Only one element is required through the depth of the plate the default number of mesh divisions must be set to one. Then will be defined translation volume of the surface. The translation direction is Z and its value 2.8mm. Now we assign the volume with mesh dataset

Composite Brick (HX16L), this element descriptions are generic element type (Structural Composite), element shape (Hexahedral), interpolation order (Quadratic). The sixteen-node brick element is shown in Figure 4.2.

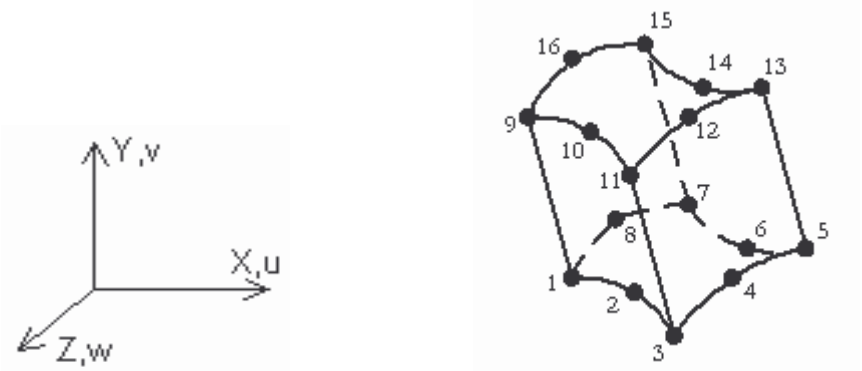

Figure 4.2 Sixteen-node brick element

Enter these knowledge, then use CTRL and A keys together select whole model and assign the composite brick dataset. After that, the element axis of the model oriented to lie along the global X axis.

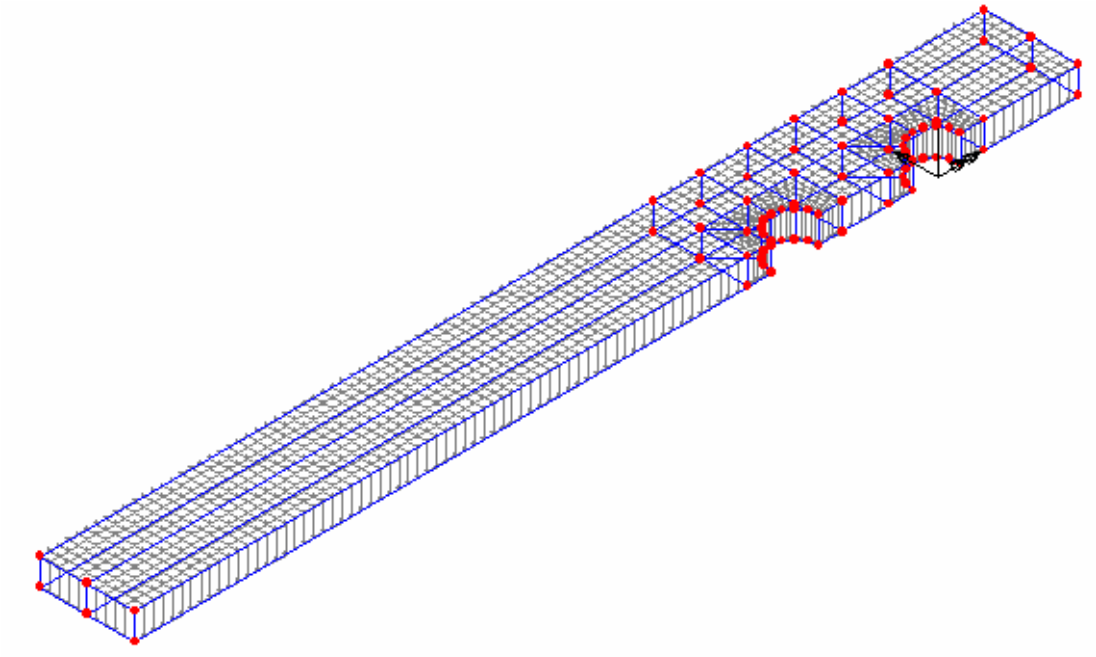

Figure 4.3 Meshing of the model

In this part of the study we will define material properties. First of all, orthotropic material was chosen, the mechanical properties of glass-vinylester composite

material was added composite library, leave the units N, mm, t, C, s. 3D solid is chosen and the option to output parameters was selected for the Hashin Damage model. Mechanical properties of glass-vinylester composite material and mechanical properties of Hashin Damage model were shown in Table 3-1. In conclusion composite laminate was defined, then CTRL and A keys were used together whole model was selected and assigned, the element axis was selected and click OK to finish this part of the study.

In this part of the study, we will see support conditions of the model. Firstly, the bottom surfaces of the half model are supported on symmetry XZ plane as shown in Figure 4.4.

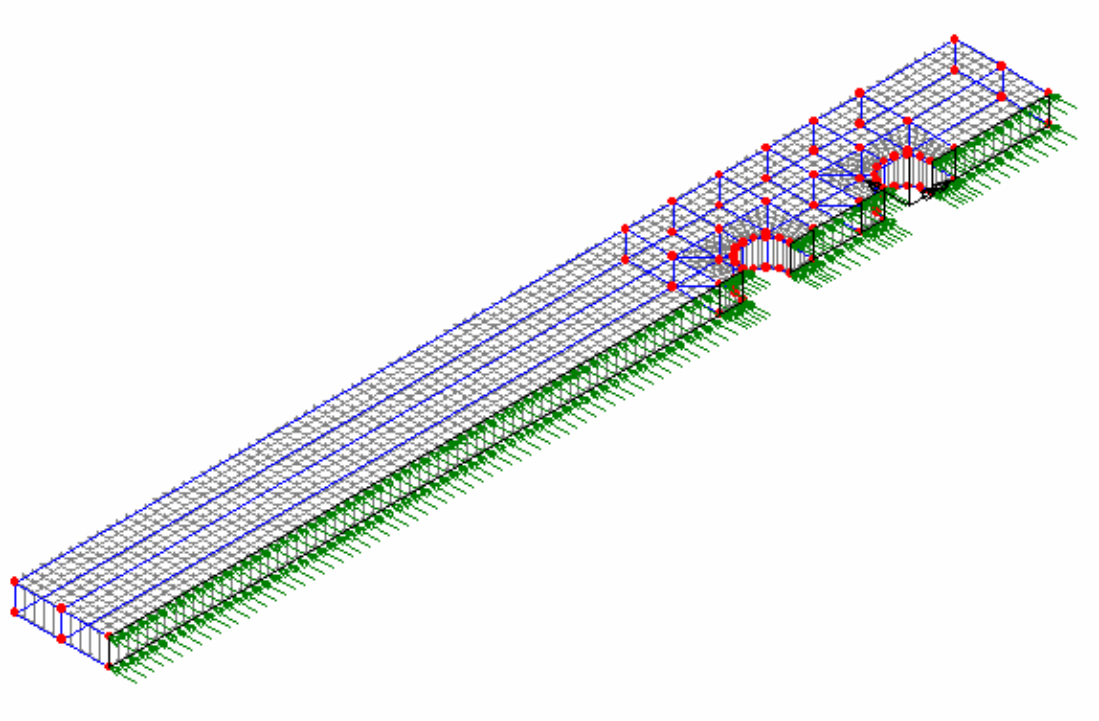

Figure 4.4 Supported surfaces on Symmetry XZ plane

Secondly, cylindrical axes are carried out two surfaces on semi cylinders. These surfaces of the plate are supported in X direction as shown in Figure 4.5.

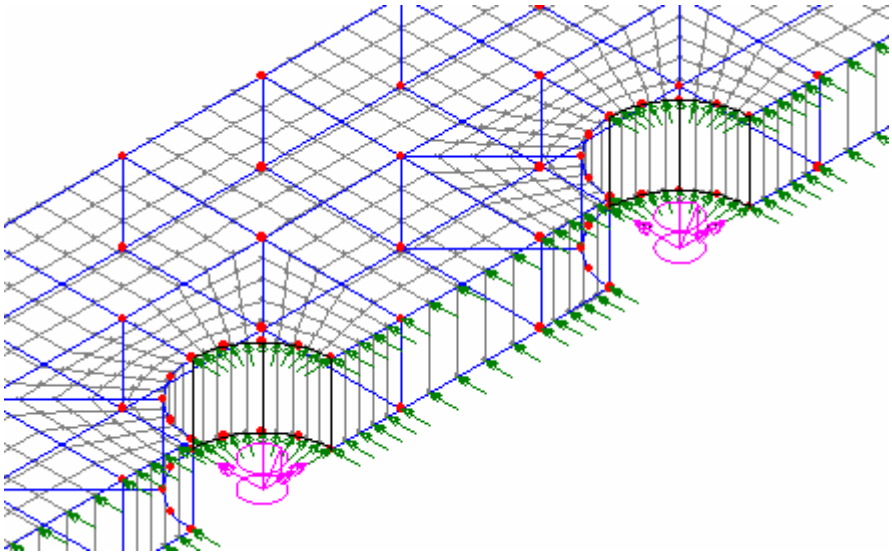

Figure 4.5 Supported surfaces in X direction with respect to cylindrical axes

Tensile load is carried out one by one per unit surface as shown in Figure 4.6.

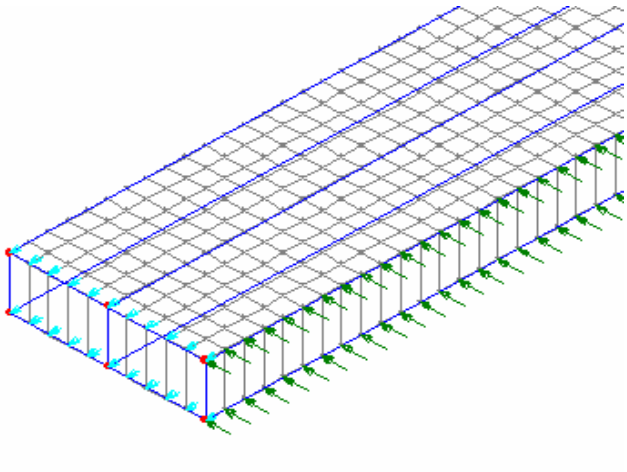

Figure 4.6 Tensile Load Direction

At the end of the numerical study, the load increment strategy needs to be defined at nonlinear solution.

CHAPTER FIVE
RESULTS AND DISCUSSION

In this study the bearing strength and failure modes are calculated experimentally and numerically. The specimens for each W/D, E/D and K/D ratio are tested for experimental analysis. Hashin criterion is used for numerical calculation. Bearing strength values and failure modes are investigated as a function of three variables, W/D ratio (2,3,4,5), E/D ratio (1,2,3,4,5) and K/D ratio (2,3,4,5). Orientation angle of fiber, $\theta = 0°$, is used in this study.

In the experimental study, it is observed that, the load/ displacement curves are linear before the initial failure. After that, the load increment is smaller than displacement increment. Generally, the load is reached the maximum value between 2 mm and 6 mm. After this point, the load decreases with increasing deformations. But the specimens continued to sustain to loading. Sometimes the highest load occurs after this event.

When edge distance to diameter ratio (E/D), width to diameter ratio (W/D) and distance between two holes to diameter ratio (K/D) are increased, the failure load reaches higher values. When E/D ratio is 1 for W/D=2 and 3, generally, the plate tear immediately before displacement is reached to 3 mm. The bearing strength values obtained are close to each other for E/D=4 and E/D=5 ratios.

The plate is the weakest for W/D=2 and the critical W/D ratio is 3. As the width of the specimen increases, the failure mode also changes to bearing mode. In addition, when K/D ratio is 2, failure load is reached lower value than the other specimens. In most of the specimens, maximum failure load is reached after first failure load with the effect of increasing K/D ratio.

The load-displacement curves of the experimental study can be seen that following figure 5.1 to figure 5.4 while W/D and E/D are kept constants.

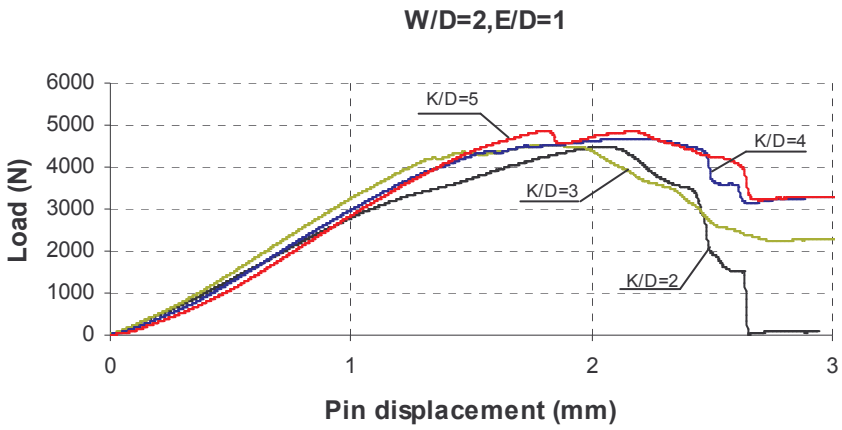
W/D=2,E/D=1
Load (N)
6000
5000
4000
3000
2000
1000
0
0
1
2
3
Pin displacement (mm)
K/D=5
K/D=4
K/D=3
K/D=2

(a)

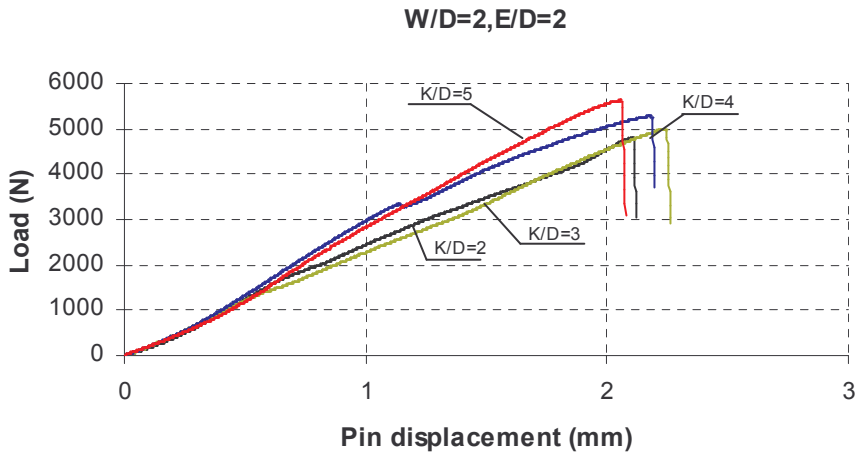
W/D=2,E/D=2
Load (N)
6000
5000
4000
3000
2000
1000
0
0
1
2
3
Pin displacement (mm)
K/D=5
K/D=4
K/D=3
K/D=2

(b)

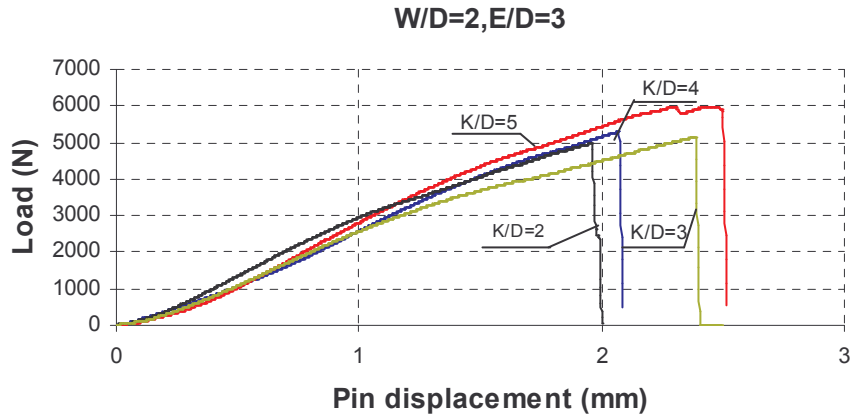
W/D=2,E/D=3
Load (N)
7000
6000
5000
4000
3000
2000
1000
0
0
1
2
3
Pin displacement (mm)
K/D=4
K/D=5
K/D=2
K/D=3

(c)

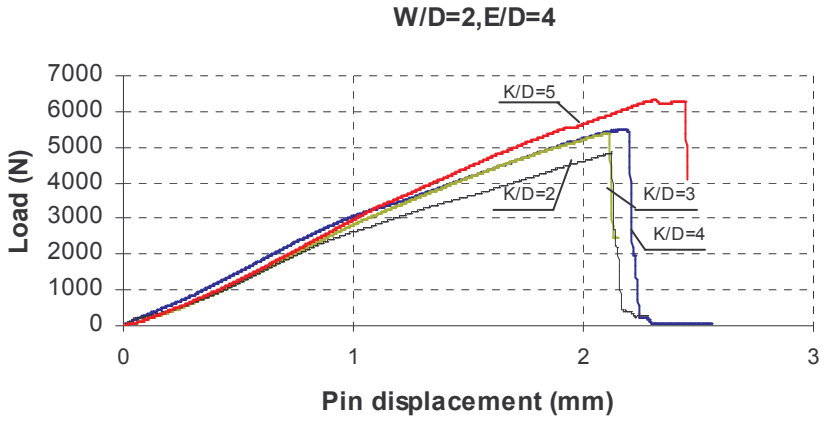

(d)

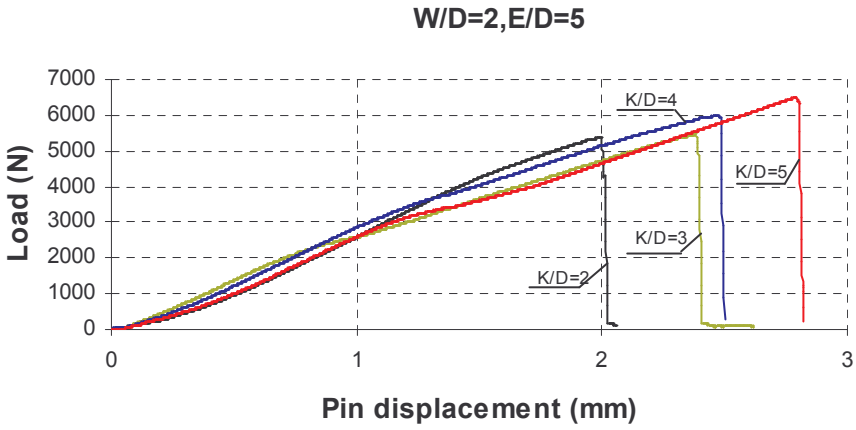

(e)

Figure 5.1 Load-displacement curves for pin-loaded glass-vinylester composite plates (W/D=2,K/D=2,3,4,5) a) E/D=1, b) E/D=2, c) E/D=3, d) E/D=4, e) E/D=5

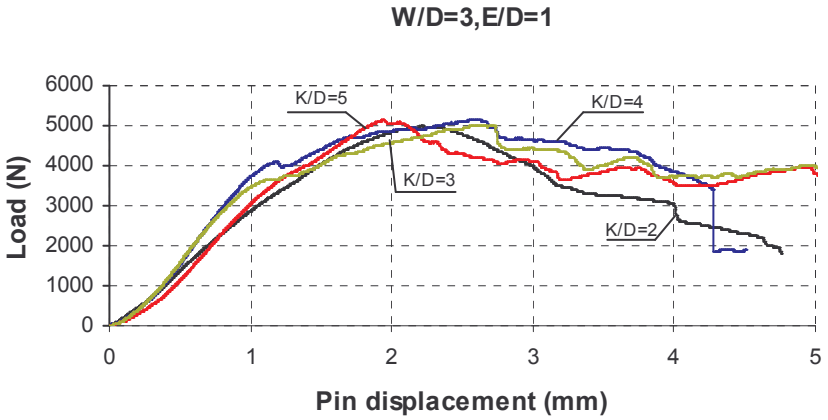
W/D=3,E/D=1
Load (N)
Pin displacement (mm)
K/D=5
K/D=4
K/D=3
K/D=2
0
1000
2000
3000
4000
5000
6000
0
1
2
3
4
5

(a)

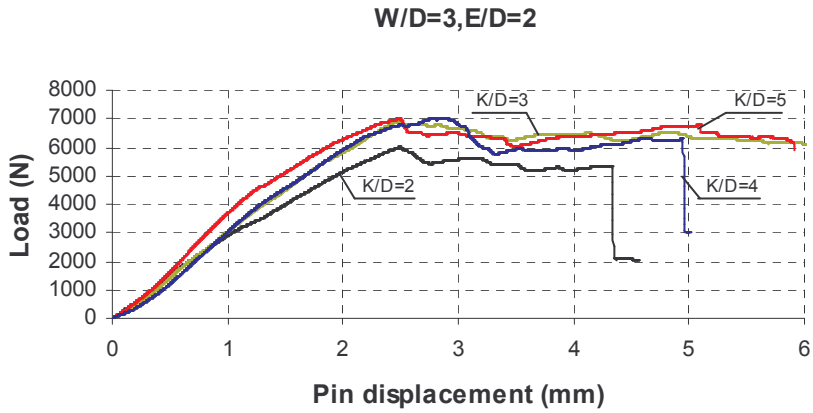
W/D=3,E/D=2
Load (N)
Pin displacement (mm)
K/D=3
K/D=5
K/D=2
K/D=4
0
1000
2000
3000
4000
5000
6000
7000
8000
0
1
2
3
4
5
6

(b)

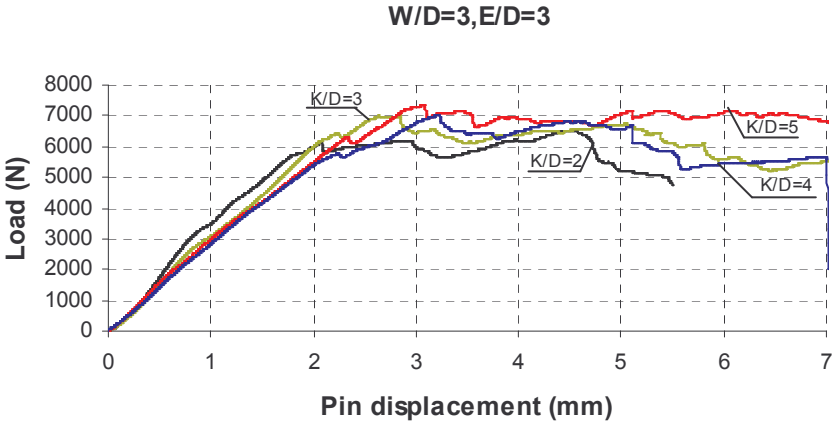
W/D=3,E/D=3
Load (N)
Pin displacement (mm)
K/D=3
K/D=5
K/D=2
K/D=4
0
1000
2000
3000
4000
5000
6000
7000
8000
0
1
2
3
4
5
6
7

(c)

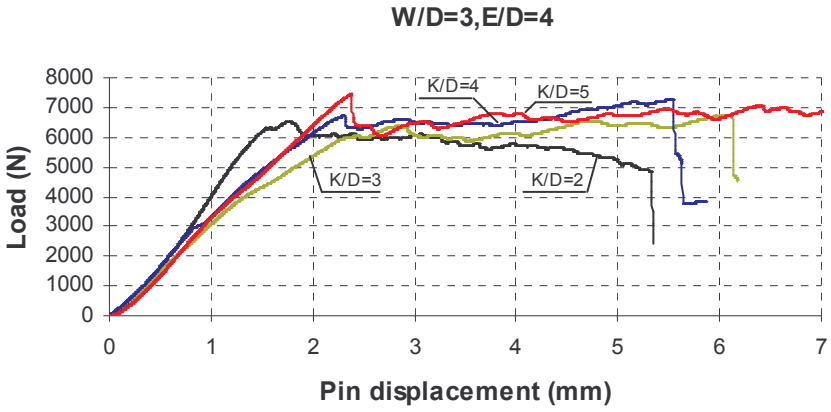

(d)

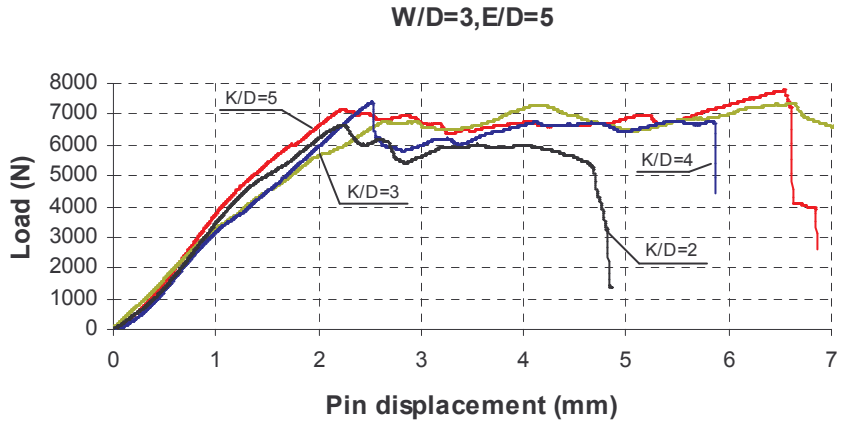

(e)

Figure 5.2 Load-displacement curves for pin-loaded glass-vinylester composite plates (W/D=3, K/D=2,3,4,5) a) E/D=1, b) E/D=2, c) E/D=3, d) E/D=4, e) E/D=5

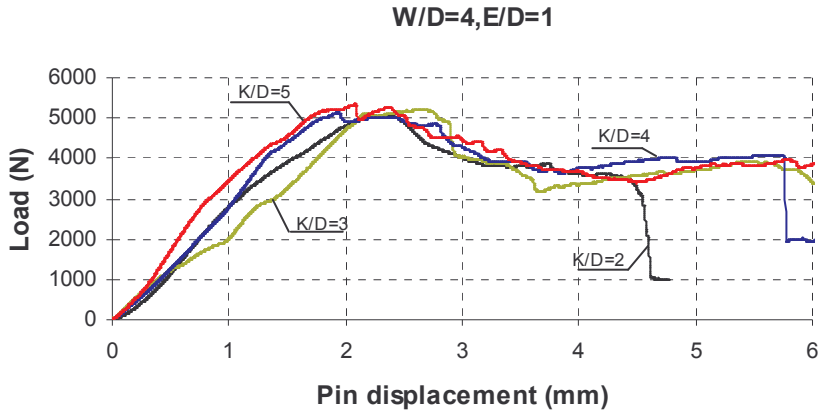
W/D=4,E/D=1
Load (N)
Pin displacement (mm)
K/D=5
K/D=4
K/D=3
K/D=2
0
1000
2000
3000
4000
5000
6000
0
1
2
3
4
5
6

(a)

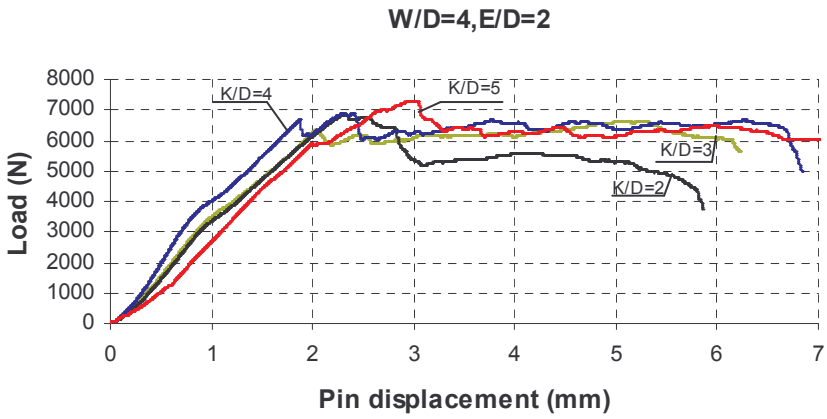
W/D=4,E/D=2
Load (N)
Pin displacement (mm)
K/D=4
K/D=5
K/D=3
K/D=2
0
1000
2000
3000
4000
5000
6000
7000
8000
0
1
2
3
4
5
6
7

(b)

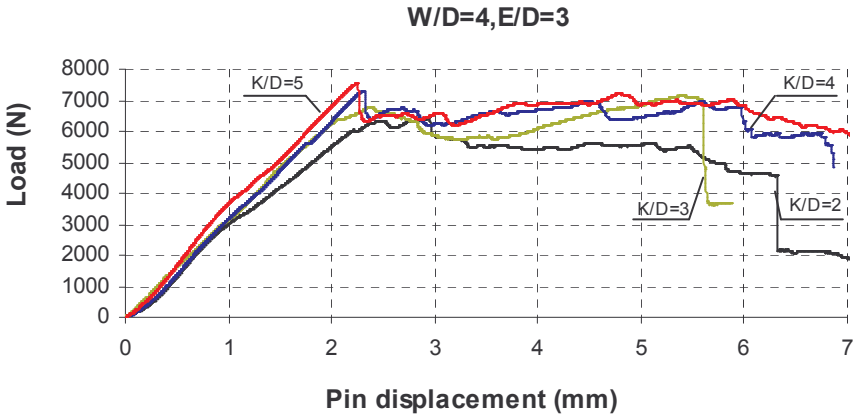
W/D=4,E/D=3
Load (N)
Pin displacement (mm)
K/D=5
K/D=4
K/D=3
K/D=2
0
1000
2000
3000
4000
5000
6000
7000
8000
0
1
2
3
4
5
6
7

(c)

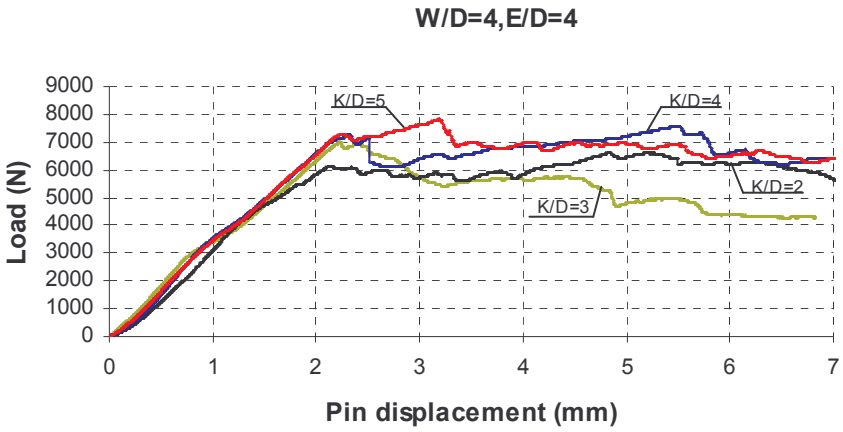

(d)

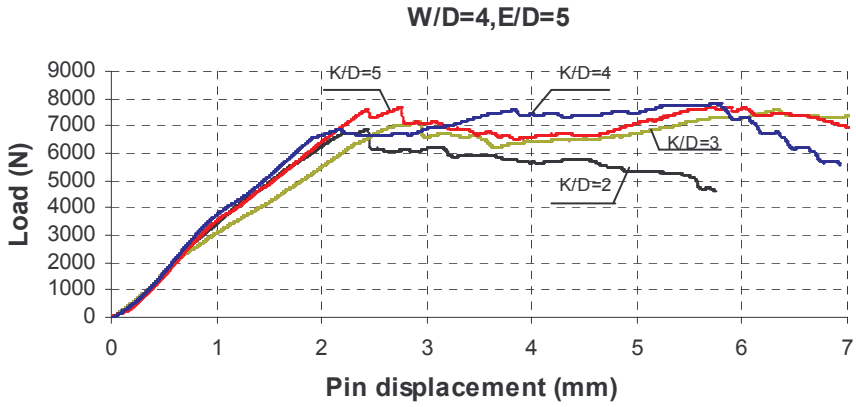

(e)

Figure 5.3 Load-displacement curves for pin-loaded glass-vinylester composite plates (W/D=2,K/D=2,3,4,5) a) E/D=1, b) E/D=2, c) E/D=3, d) E/D=4, e) E/D=5

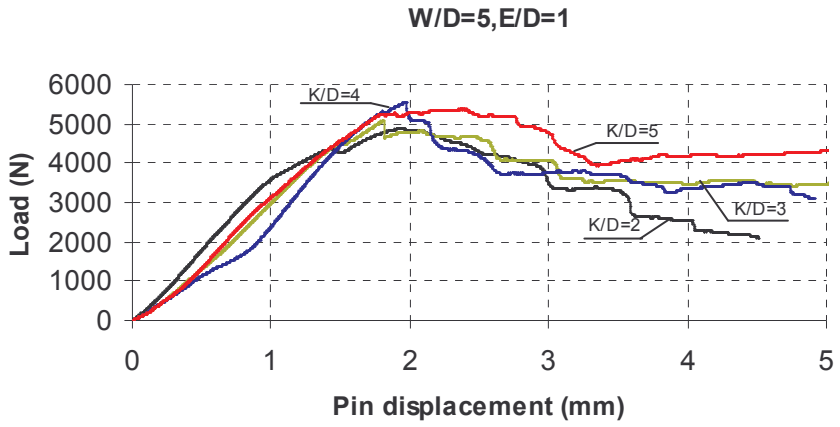
W/D=5,E/D=1
Load (N)
Pin displacement (mm)
K/D=4
K/D=5
K/D=3
K/D=2
0
1000
2000
3000
4000
5000
6000
0
1
2
3
4
5

(a)

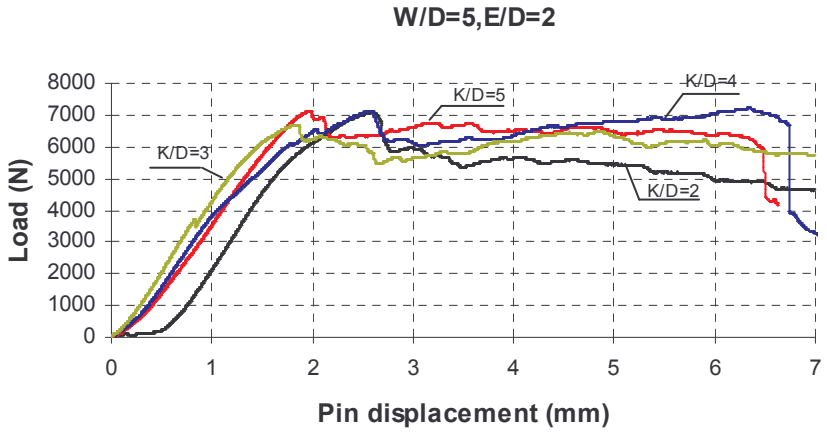
W/D=5,E/D=2
Load (N)
Pin displacement (mm)
K/D=4
K/D=5
K/D=3
K/D=2
0
1000
2000
3000
4000
5000
6000
7000
8000
0
1
2
3
4
5
6
7

(b)

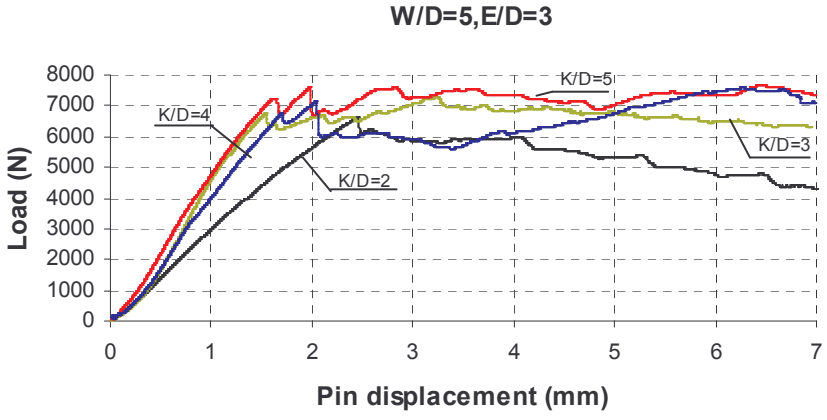
W/D=5,E/D=3
Load (N)
Pin displacement (mm)
K/D=5
K/D=4
K/D=3
K/D=2
0
1000
2000
3000
4000
5000
6000
7000
8000
0
1
2
3
4
5
6
7

(c)

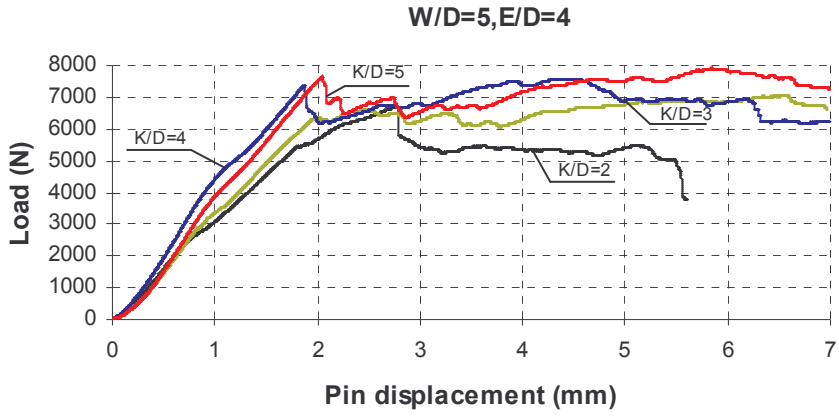

(d)

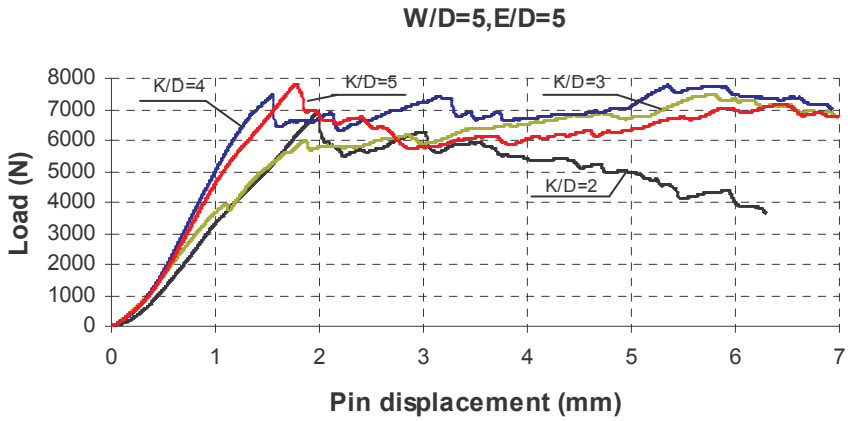

(e)

Figure 5.4 Load-displacement curves for pin-loaded glass-vinylester composite plates (W/D=2, K/D=2,3,4,5) a) E/D=1, b) E/D=2, c) E/D=3, d) E/D=4, e) E/D=5

The bearing strength values are highly dependent on E/D ratio. There is a decrease in the bearing strength as E/D approaches 1, which indicates that the hole is too close to the specimen edge to adequately support the load. Generally, while the W/D and K/D ratios are constant, bearing strength values increase with increasing E/D ratio. The plate is the weakest for E/D=1. The change in types of failure helps to explain why there are transition regions in the graphs of Figure 5.5 and Figure 5.8 at E/D=1 to 5. At low values of E/D, the failure types are net-tension or shear-out which is weak type of failure, and high values of E/D, the failure type is bearing which is better mode of resisting load in Table 5.1-4.

Bearing strength increases with increasing K/D ratio, while E/D and W/D ratios are constant. In spite of failure occurs at first hole, loading goes on with the effect of K/D ratio. The change in types of failure helps to explain why there are transition regions in the graphs of Figure 5.7 and Figure 5.10 at K/D=2 to 5.

Pin bearing strength decreases with decreasing W/D ratio, while E/D and K/D ratios are constant. The plate is the weakest for W/D=2. Generally, bearing failure mode occurs at the specimens of W/D>3.The change in types of failure helps to explain why there are transition regions in the graphs of Figure 5.6 and Figure 5.9 at W/D=2 to 5. As the width of the specimen increases, there is a point where the mode of failure changes to bearing in Table 5.1-4.

At the end of this chapter, the results of numerical study for Hashin criteria are shown Figure 5.11 to Figure 5.22. In addition, maximum failure load and failure mode are shown in these figures.

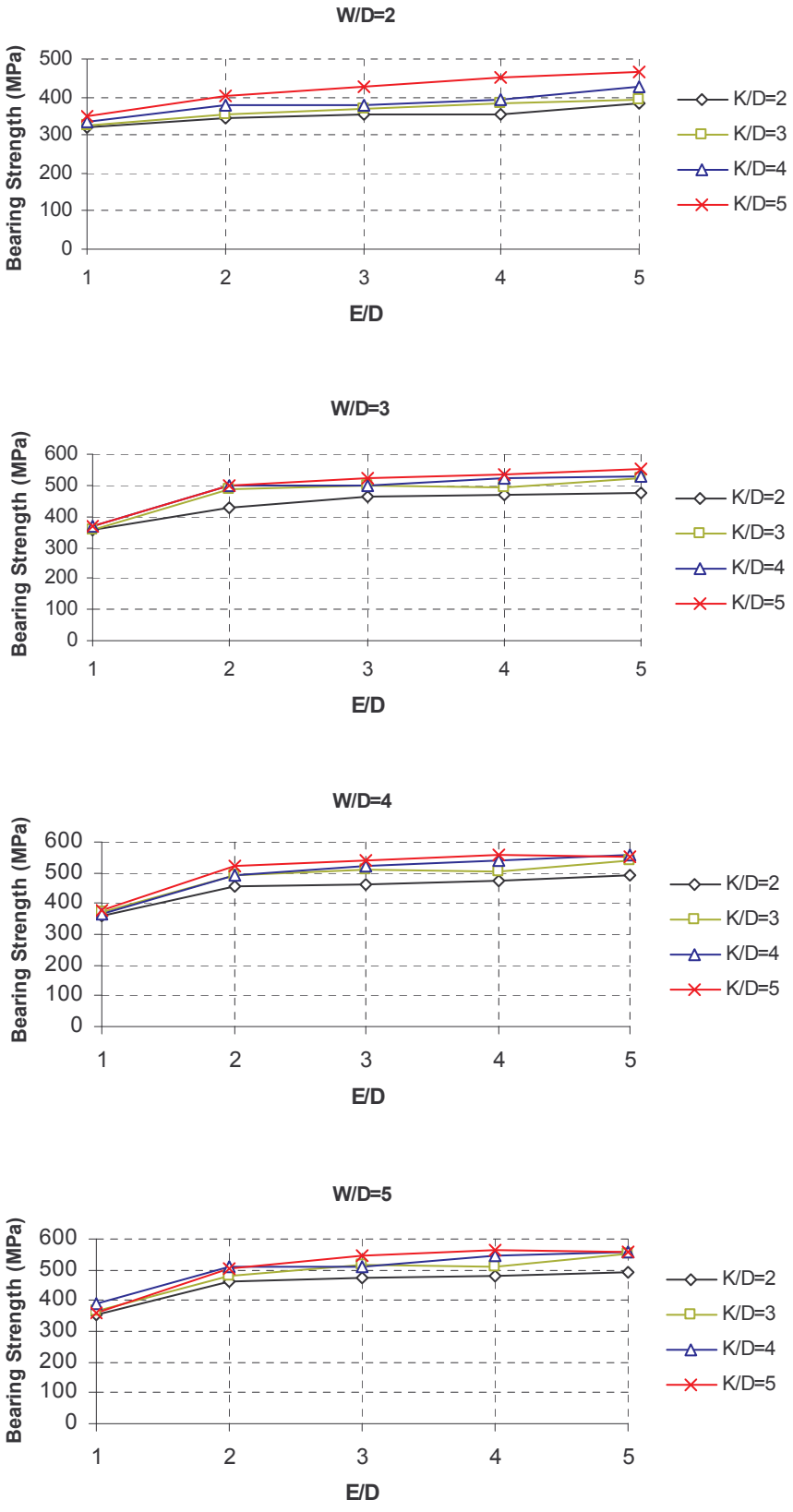

Figure 5.5 The effect of E/D ratio according to (K/D=2,3,4,5) on the bearing strength for (W/D=2,3,4,5) in experimental study

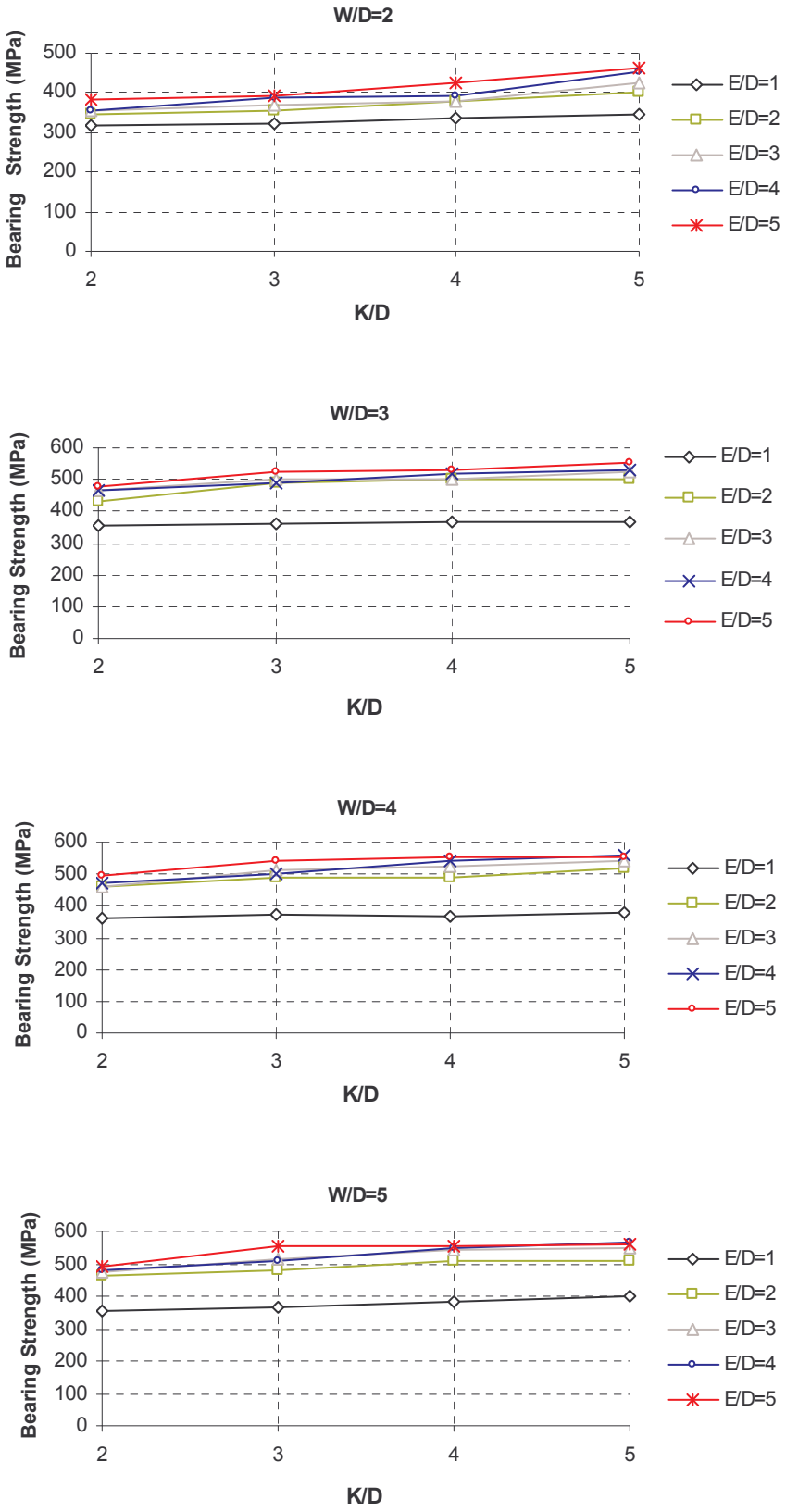

Figure 5.6 The effect of E/D ratio according to (K/D=2,3,4,5) on the bearing strength for (W/D=2,3,4,5) in experimental study

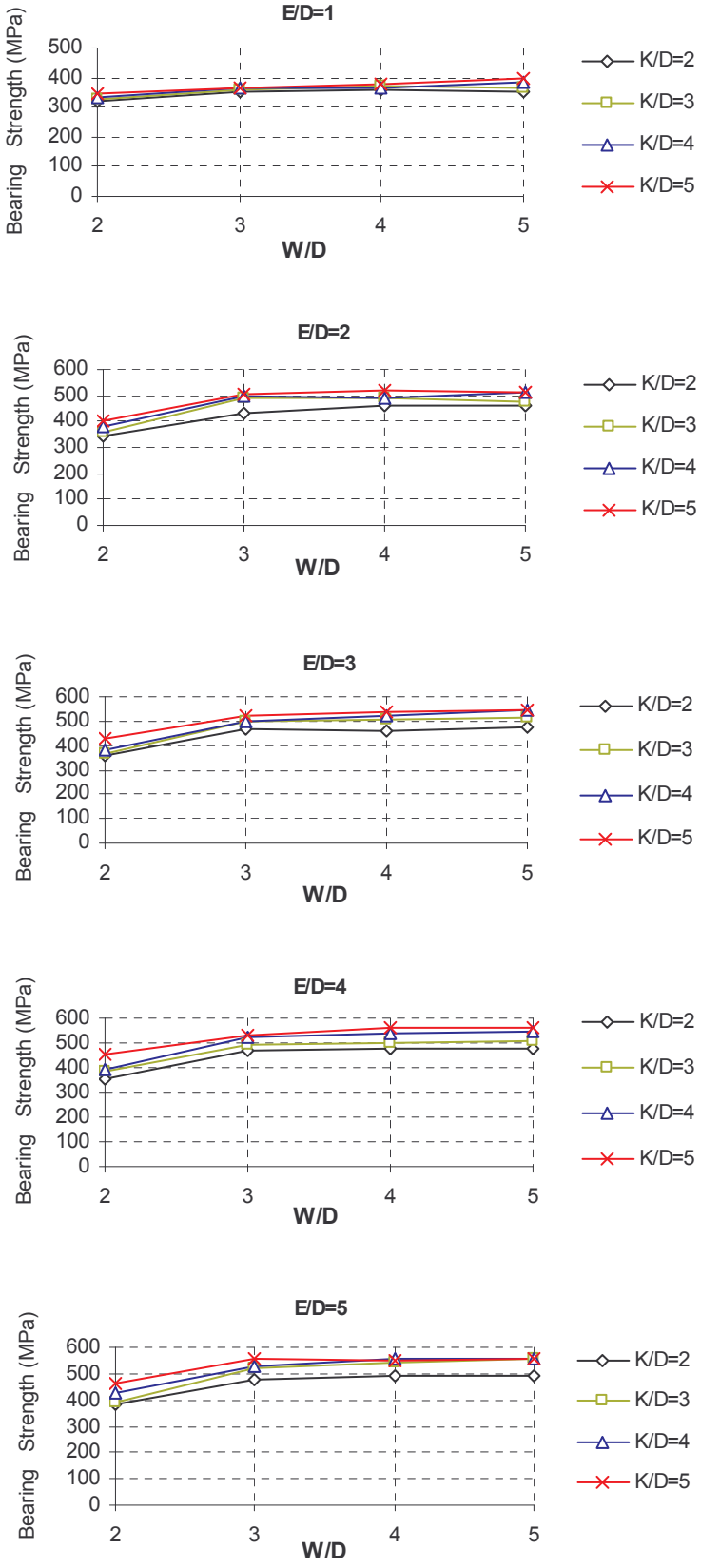

Figure 5.7 The effect of E/D ratio according to (K/D=2,3,4,5) on the bearingstrength for (W/D=2,3,4,5) in experimental study

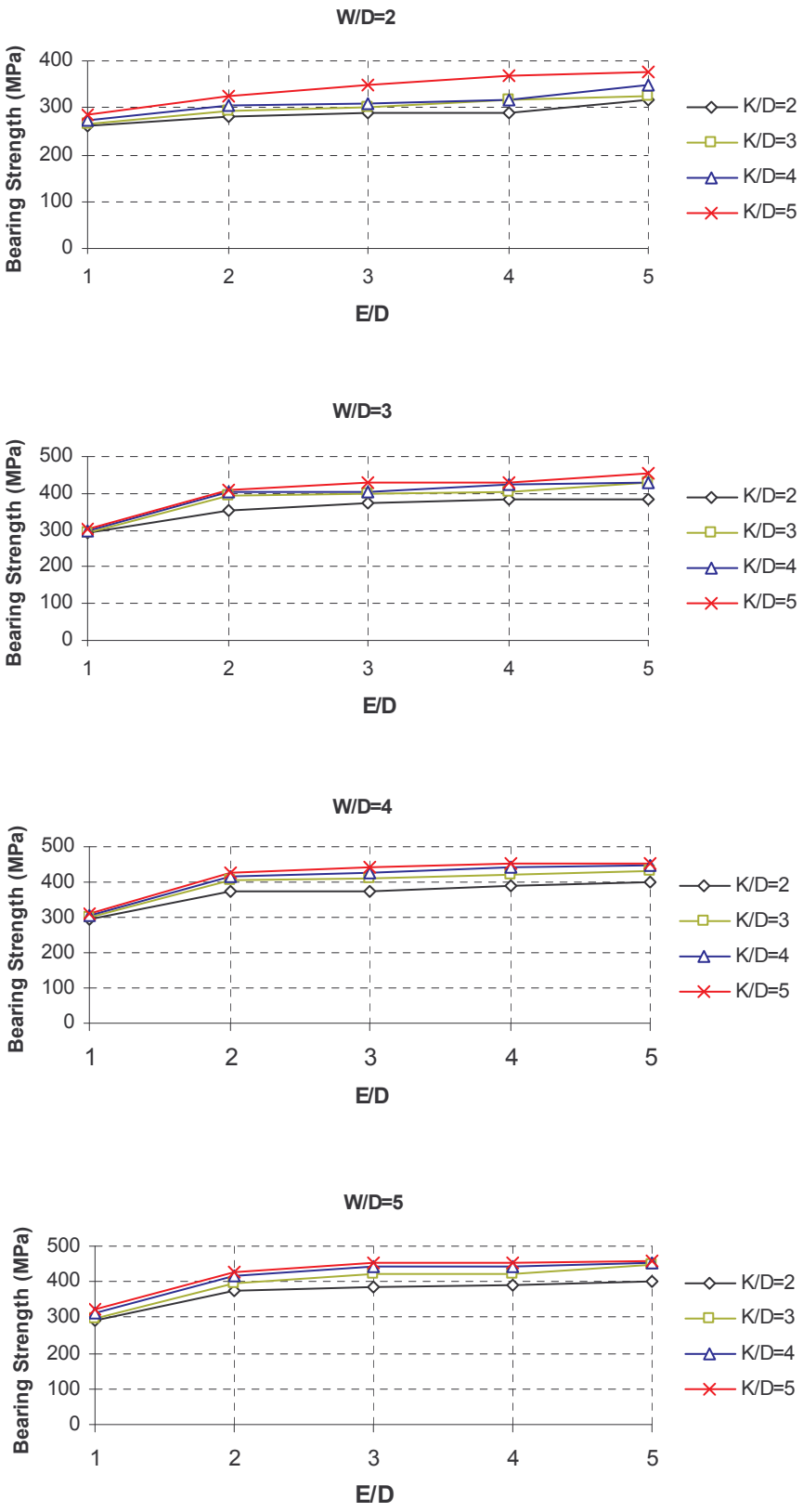

Figure 5.8 The effect of E/D ratio according to (K/D=2,3,4,5) on the bearing strength for (W/D=2,3,4,5) in experimental study

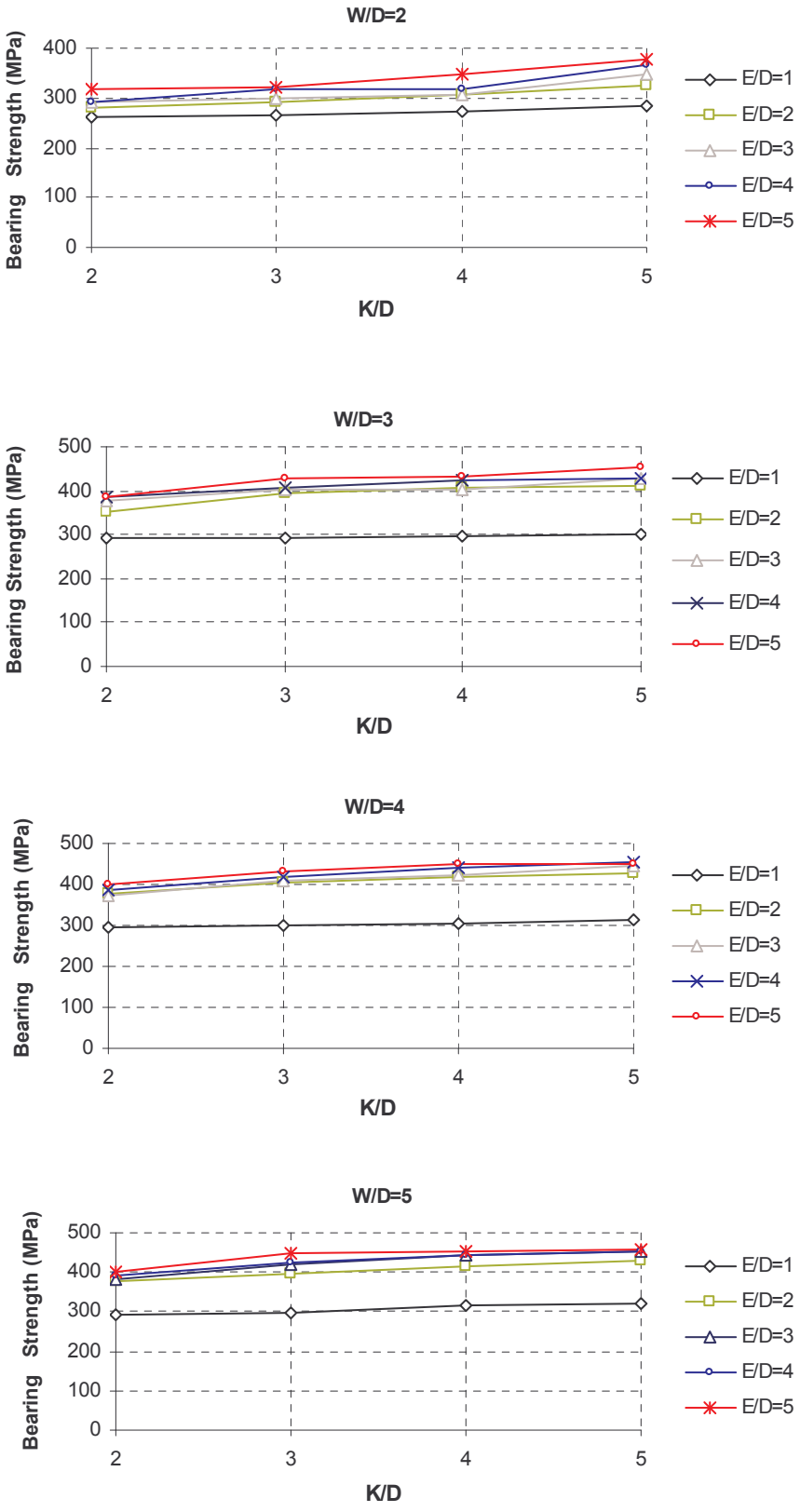

Figure 5.9 The effect of E/D ratio according to (K/D=2,3,4,5) on the bearing strength for (W/D=2,3,4,5) in experimental study

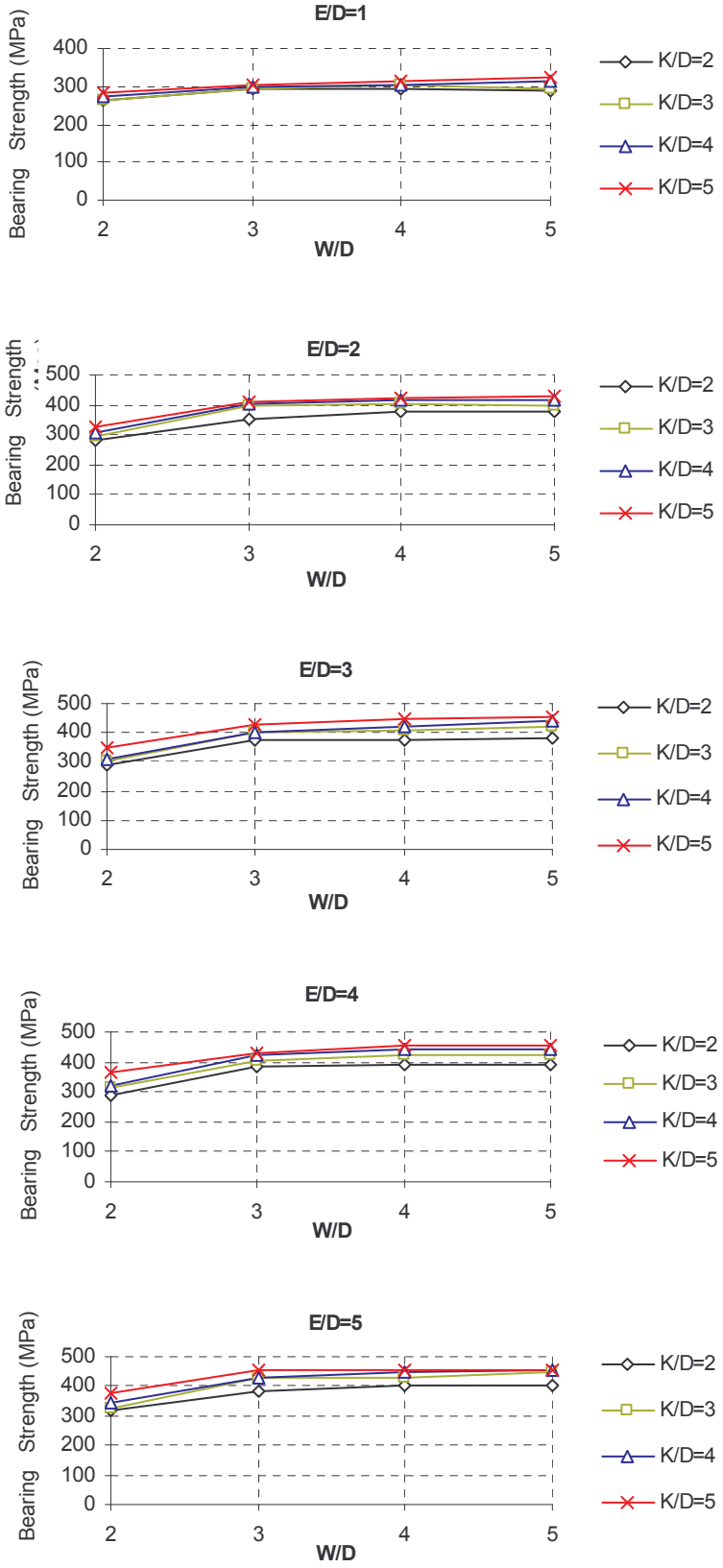

Figure 5.10 The effect of E/D ratio according to (K/D=2,3,4,5) on the bearing strength for (W/D=2,3,4,5) in experimental study

Table 5.1 Comparisons of experimental and numerical failure modes and loads for W/D=2 specimens.(B=bearing mode, S= shear-out mode, N= net-tension mode)

W/D=2		Failure Mode		Failure Load (N)		Bearing Strength (Mpa)	
		Exp.	**Hashin**	**Exp.**	**Hashin**	**Exp.**	**Hashin**
E/D=1	K/D=2	N	N	4475	3700	319	264
	K/D=3	N	N	4534	3720	323	265
	K/D=4	N	N	4678	3800	334	271
	K/D=5	N	N	4861	3980	347	284
E/D=2	K/D=2	N	N	4822	3920	344	280
	K/D=3	N	N	4986	4100	356	292
	K/D=4	N	N	5278	4280	377	305
	K/D=5	N	N	5629	4560	402	325
E/D=3	K/D=2	N	N	4988	4060	356	290
	K/D=3	N	N	5166	4200	369	300
	K/D=4	N	N	5309	4300	379	307
	K/D=5	S-N	N	5985	4860	427	347
E/D=4	K/D=2	N	N	4986	4060	356	290
	K/D=3	N	N	5397	4440	385	317
	K/D=4	S-N	N	5492	4460	392	318
	K/D=5	S-N	N	6328	5140	452	367
E/D=5	K/D=2	N	N	5395	4440	385	317
	K/D=3	N	N	5476	4520	391	322
	K/D=4	S-N	N	5979	4860	427	347
	K/D=5	S-N	N	6504	5280	464	377

Table 5.2 Comparisons of experimental and numerical failure modes and loads for W/D=3 specimens.(B=bearing mode, S= shear-out mode, N= net-tension mode)

W/D=3		Failure Mode		Failure Load (N)		Bearing Strength (Mpa)	
		Exp.	Hashin	Exp.	Hashin	Exp.	Hashin
E/D=1	K/D=2	N	S-N	4979	4100	355	292
	K/D=3	S-N	S-N	5020	4100	358	292
	K/D=4	S	S-N	5140	4180	367	298
	K/D=5	S	S-N	5154	4220	368	301
E/D=2	K/D=2	S-N	S-N	6010	4920	429	351
	K/D=3	S-N	S	6818	5520	487	394
	K/D=4	S	S	6998	5680	499	405
	K/D=5	S	S	7026	5740	501	410
E/D=3	K/D=2	S-N	S	6527	5260	466	375
	K/D=3	S	S	6997	5620	499	401
	K/D=4	S	S	7020	5680	501	405
	K/D=5	S	S	7352	5980	525	427
E/D=4	K/D=2	B-S-N	S	6540	5400	467	385
	K/D=3	S	S	6870	5680	490	405
	K/D=4	S	B-S	7278	5960	519	425
	K/D=5	B-S	B-S	7447	6020	531	430
E/D=5	K/D=2	S	S	6647	5380	474	384
	K/D=3	S	B-S	7306	6020	521	428
	K/D=4	B-S	B-S	7392	6040	528	431
	K/D=5	B-S	B	7776	6360	555	454

Table 5.3 Comparisons of experimental and numerical failure modes and loads for W/D=4 specimens.(B=bearing mode, S= shear-out mode, N= net-tension mode)

W/D=4		Failure Mode		Failure Load (N)		Bearing Strength (Mpa)	
		Exp.	Hashin	Exp.	Hashin	Exp.	Hashin
E/D=1	K/D=2	S	S-N	5065	4120	361	294
	K/D=3	S	S	5221	4220	372	301
	K/D=4	S	S	5139	4240	367	302
	K/D=5	S	B-S-N	5332	4360	380	311
E/D=2	K/D=2	S	S-N	6407	5260	457	375
	K/D=3	B-S	S	6854	5660	489	404
	K/D=4	B-S	B-S	6881	5840	491	417
	K/D=5	B	B	7284	5960	520	425
E/D=3	K/D=2	B-S	S	6448	5240	460	374
	K/D=3	B-S	B-S	7140	5740	510	410
	K/D=4	B	B	7318	5940	522	424
	K/D=5	B	B	7562	6220	540	444
E/D=4	K/D=2	B-S	S	6636	5440	474	388
	K/D=3	B-S	B-S	7021	5880	501	420
	K/D=4	B	B	7571	6180	540	441
	K/D=5	B	B	7822	6360	558	454
E/D=5	K/D=2	B	B-S	6903	5620	493	401
	K/D=3	B	B	7587	6020	541	430
	K/D=4	B	B	7783	6300	555	450
	K/D=5	B	B	7709	6320	550	451

Table 5.4 Comparisons of experimental and numerical failure modes and loads for W/D=5 specimens.(B=bearing mode, S= shear-out mode, N= net-tension mode)

W/D=5		Failure Mode		Failure Load (N)		Bearing Strength (Mpa)	
		Exp.	Hashin	Exp.	Hashin	Exp.	Hashin
E/D=1	K/D=2	B-S	B-S	4980	4100	355	292
	K/D=3	B-S	B-S	5100	4140	364	295
	K/D=4	B-S	B	5370	4400	383	314
	K/D=5	B	B	5566	4520	397	322
E/D=2	K/D=2	B-S	B-S	6491	5280	463	377
	K/D=3	B-S	B	6703	5560	478	397
	K/D=4	B	B	7143	5820	510	415
	K/D=5	B	B	7126	5980	509	427
E/D=3	K/D=2	B-S	B	6648	5380	474	384
	K/D=3	B	B	7200	5900	514	421
	K/D=4	B	B	7590	6160	542	440
	K/D=5	B	B	7683	6320	548	451
E/D=4	K/D=2	B-S	B	6707	5460	479	390
	K/D=3	B	B	7150	5920	510	422
	K/D=4	B	B	7658	6200	547	442
	K/D=5	B	B	7909	6360	564	454
E/D=5	K/D=2	B	B	6897	5620	492	401
	K/D=3	B	B	7620	6280	544	448
	K/D=4	B	B	7776	6340	555	452
	K/D=5	B	B	7833	6400	559	457

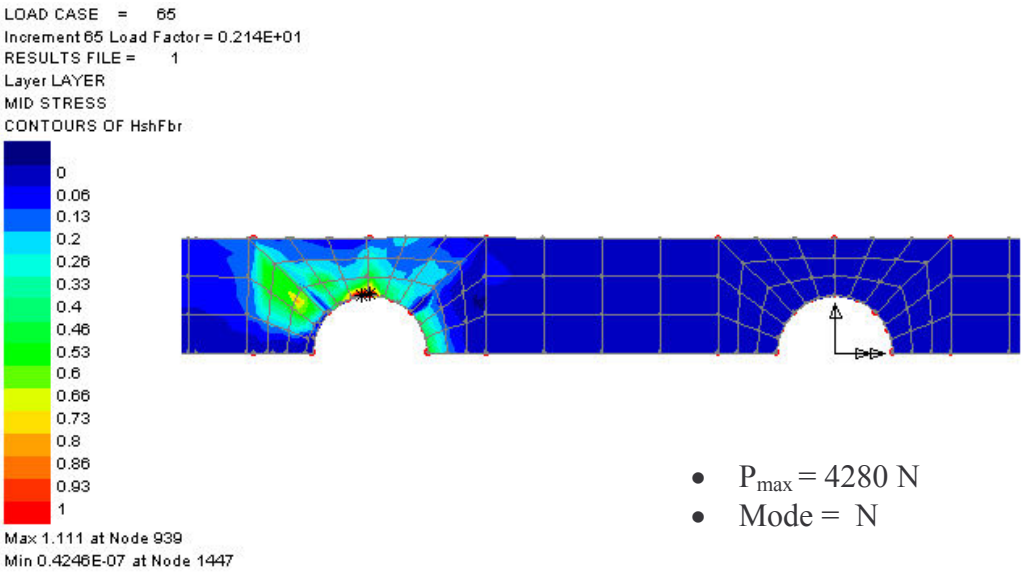

Figure 5.11 Hashin failure criteria for W/D=2, E/D=2, K/D=4 (B = bearing mode, S = shear-out mode, N = net-tension mode)

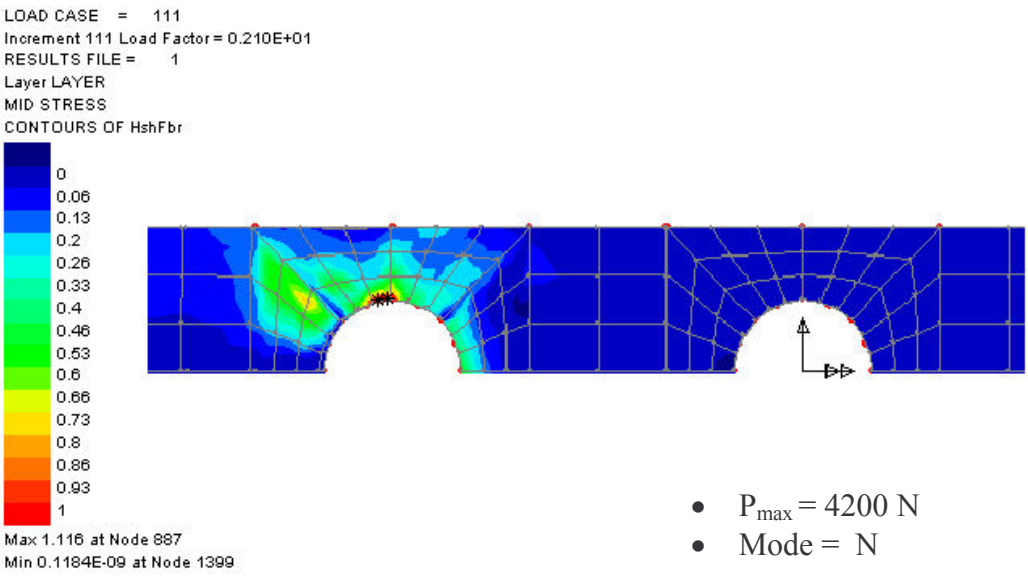

Figure 5.12 Hashin failure criteria for W/D=2, E/D=3, K/D=3 (B = bearing mode, S = shear-out mode, N = net-tension mode)

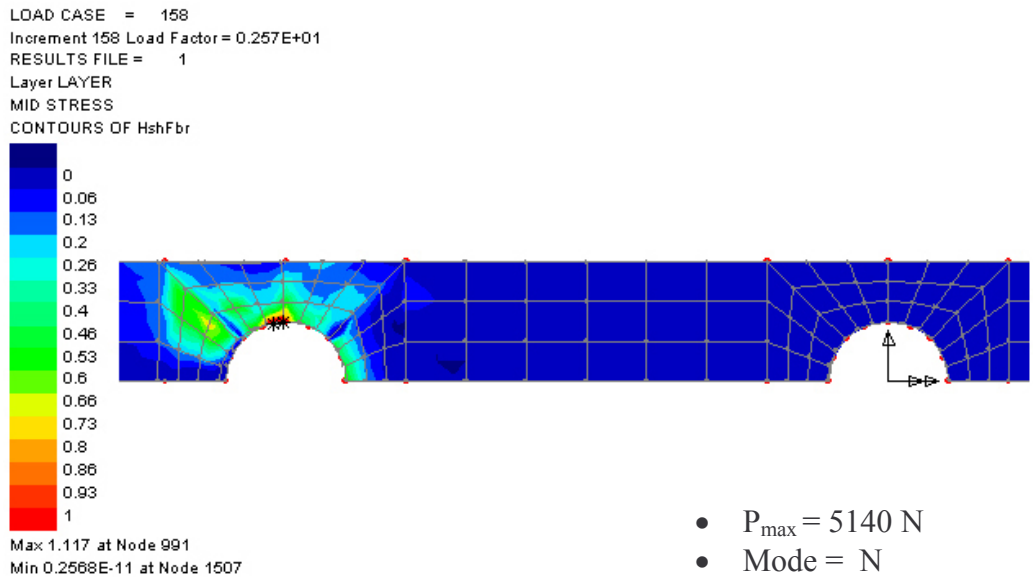

Figure 5.13 Hashin failure criteria for W/D=2, E/D=4, K/D=5 (B = bearing mode, S = shear-out mode, N = net-tension mode)

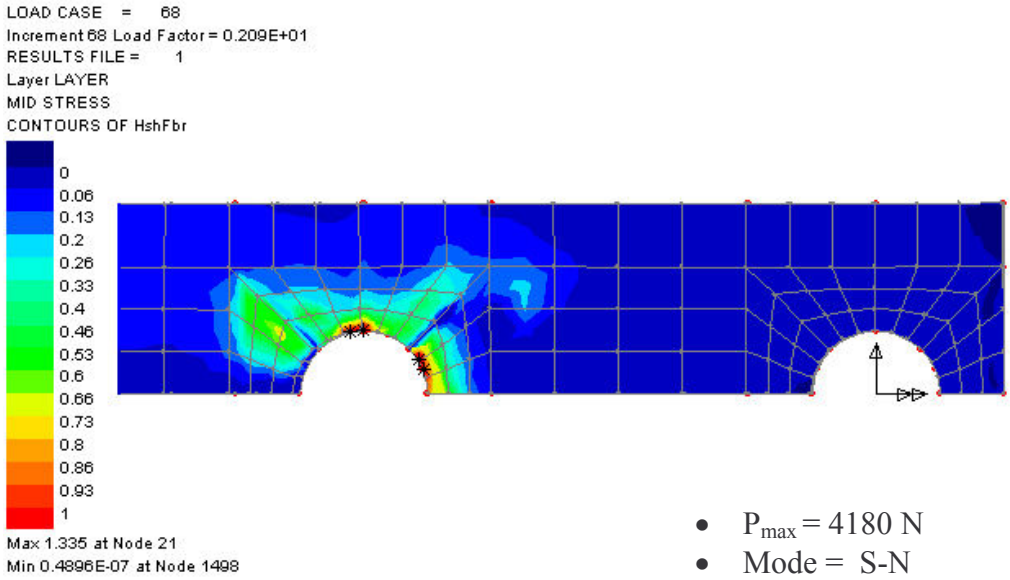

Figure 5.14 Hashin failure criteria for W/D=3, E/D=1, K/D=4 (B = bearing mode, S = shear-out mode, N = net-tension mode)

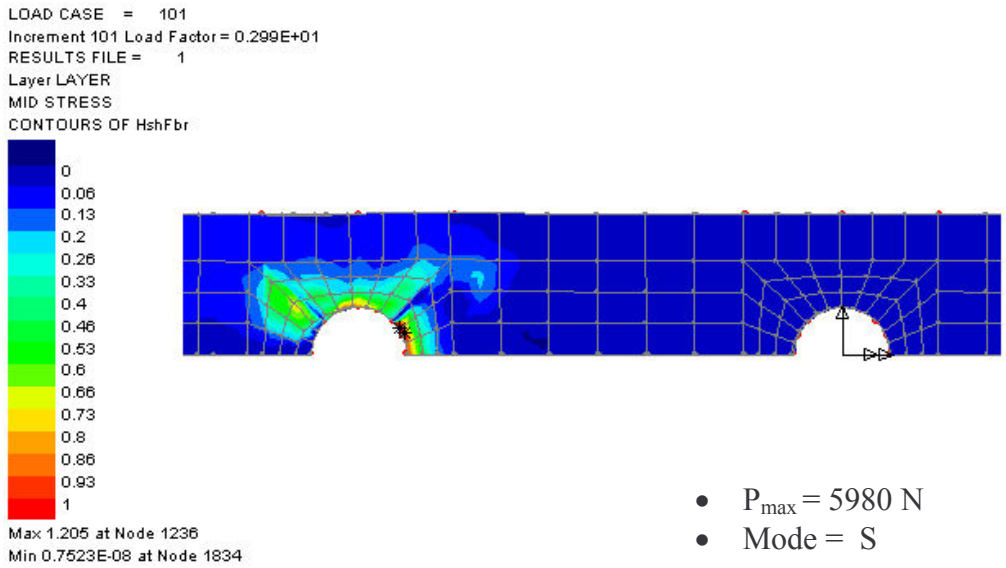

Figure 5.15 Hashin failure criteria for W/D=3, E/D=3, K/D=5 (B = bearing mode, S = shear-out mode, N = net-tension mode)

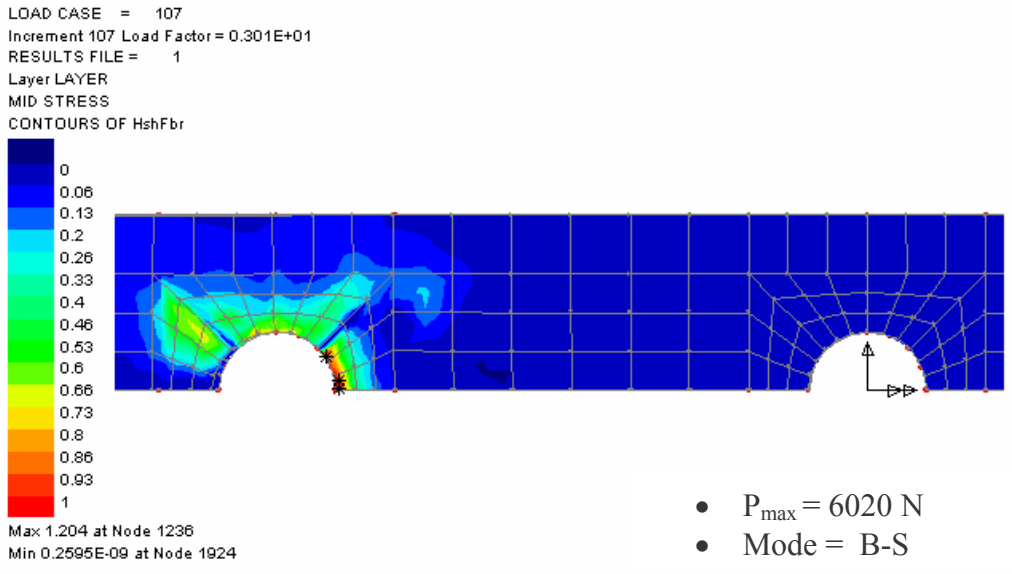

Figure 5.16 Hashin failure criteria for W/D=3, E/D=4, K/D=5 (B = bearing mode, S = shear-out mode, N = net-tension mode)

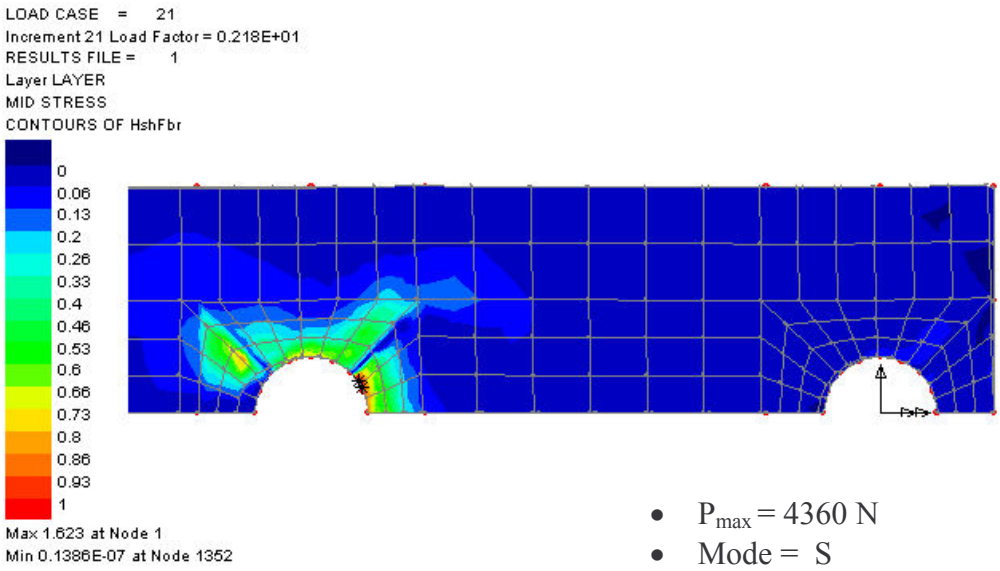

Figure 5.17 Hashin failure criteria for W/D=4, E/D=1, K/D=5 (B = bearing mode, S = shear-out mode, N = net-tension mode)

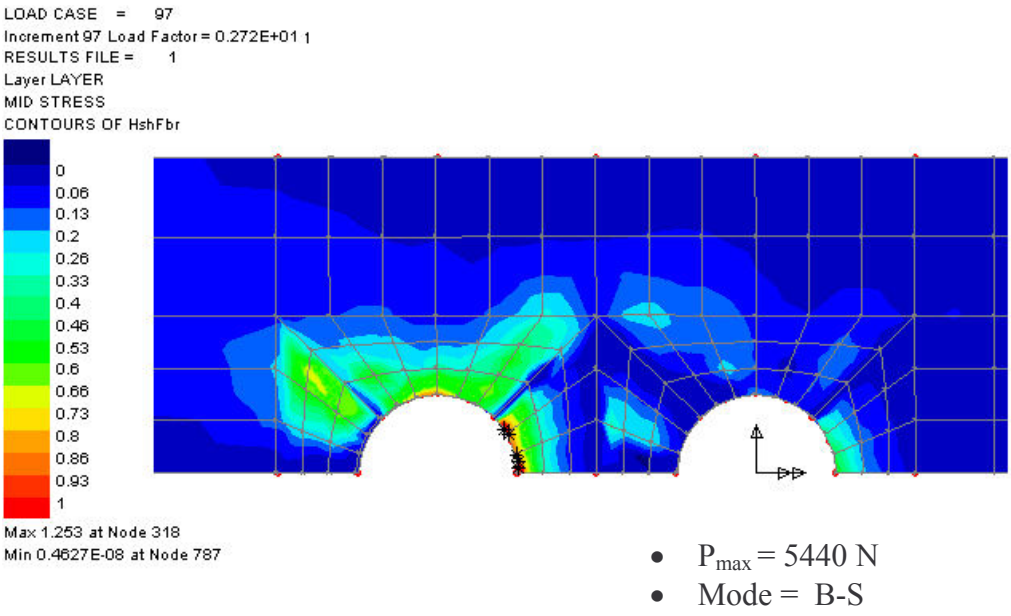

Figure 5.18 Hashin failure criteria for W/D=4, E/D=4, K/D=2 (B = bearing mode, S = shear-out mode, N = net-tension mode)

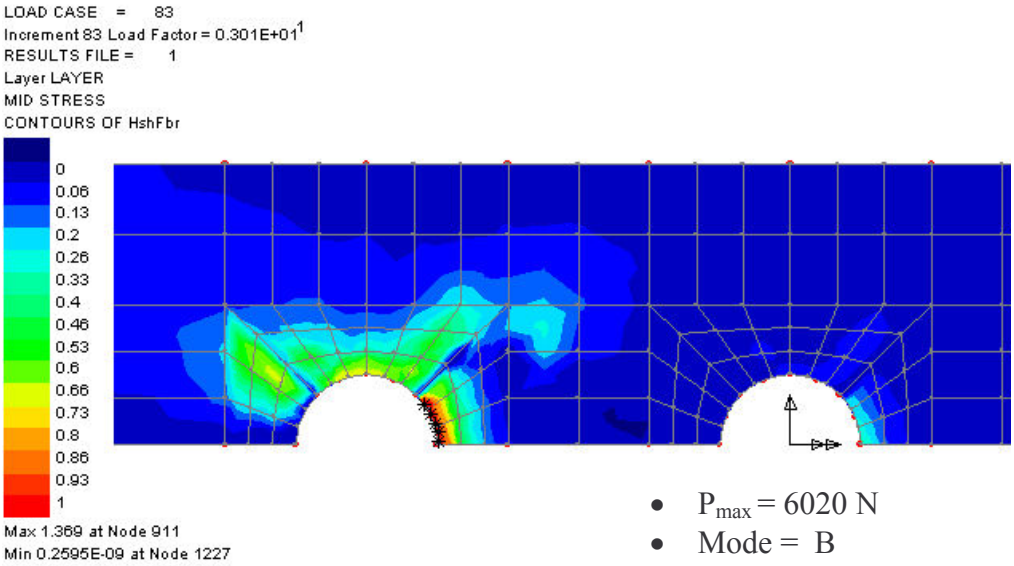

Figure 5.19 Hashin failure criteria for W/D=4, E/D=5, K/D=3 (B = bearing mode, S = shear-out mode, N = net-tension mode)

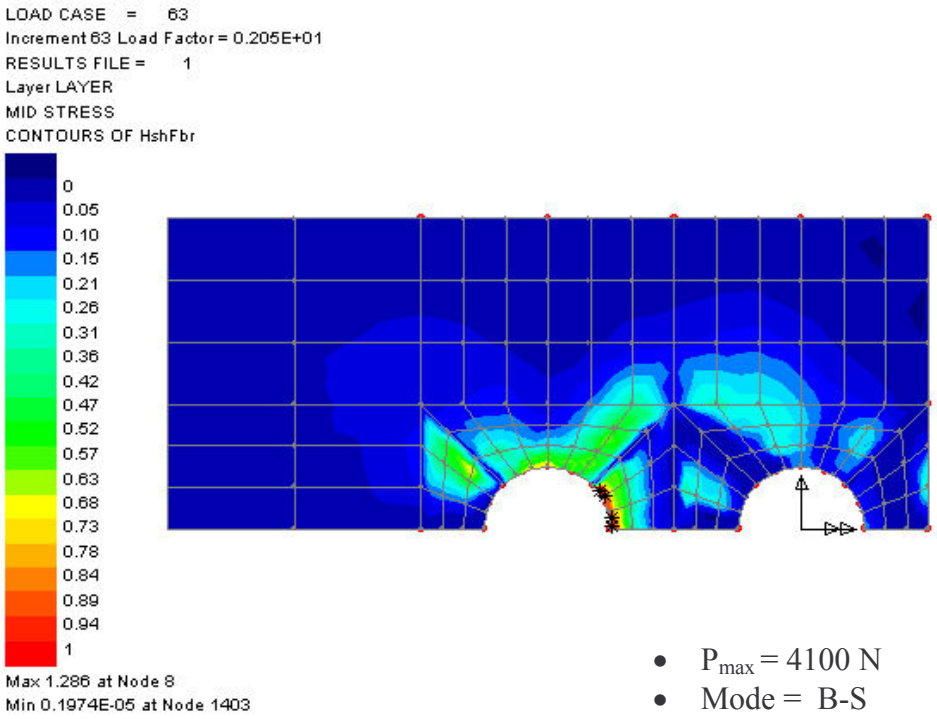

Figure 5.20 Hashin failure criteria for W/D=5, E/D=1, K/D=2 (B = bearing mode, S = shear-out mode, N = net-tension mode)

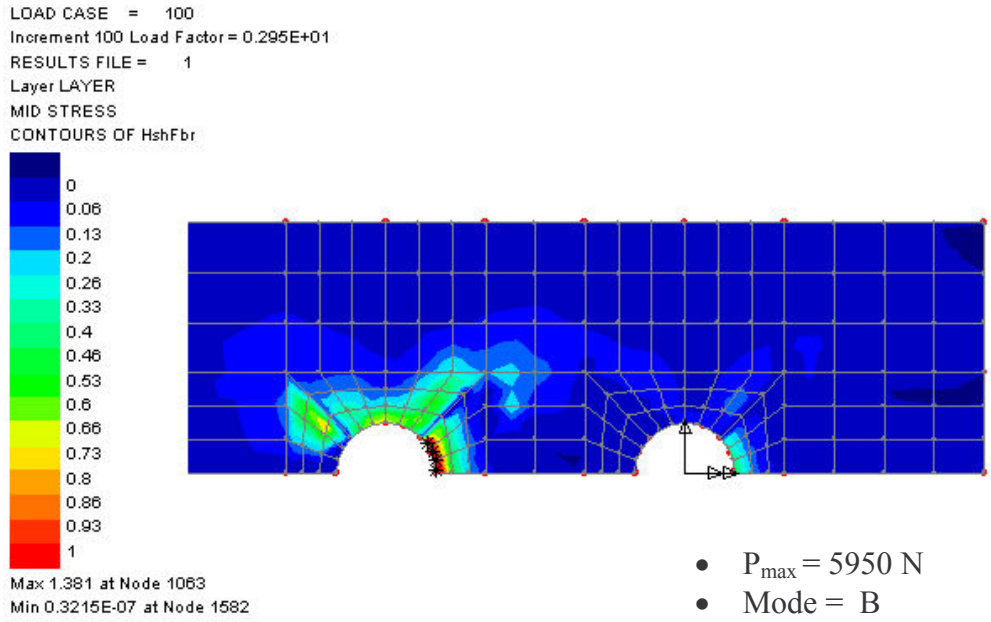

Figure 5.21 Hashin failure criteria for W/D=5, E/D=3, K/D=3 (B = bearing mode, S = shear-out mode, N = net-tension mode)

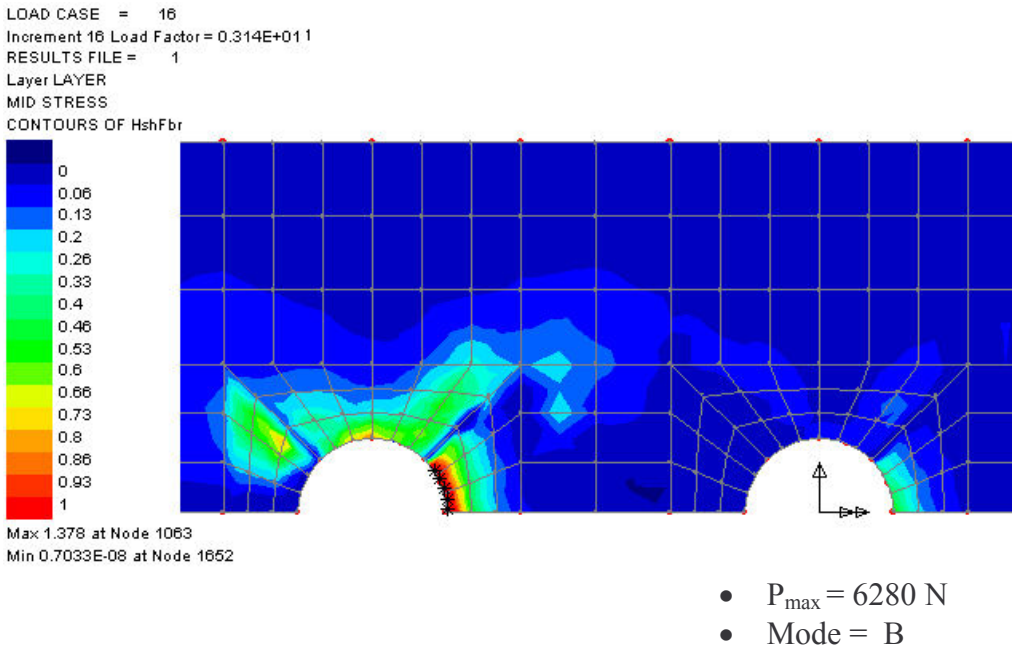

Figure 5.22 Hashin failure criteria for W/D=5, E/D=5, K/D=3 (B = bearing mode, S = shear-out mode, N = net-tension mode)

CHAPTER SIX
CONCLUSION

In this study, bearing strength, failure mode and maximum failure load in a glass-vinylester composite plate with two circular holes, which is subjected to traction force by two rigid pins, are investigated experimentally and numerically. In numerical study, Hashin criteria is used to predict the maximum failure load and failure types. The specimens for each W/D, E/D and K/D ratio are tested for experimental study. Experimental results concerning failure types and failure loads are obtained and compared with these predictions. It is seen that the results are close to each other. In addition, the effects of geometric parameters are observed. All the numerical and experimental results obtained are presented in tables and figures.

Bearing strength of the composite plate increases by going up the geometric parameters. It means that, when edge distance to diameter ratio (E/D), distance between two holes to diameter ratio (K/D) and width to diameter ratio (W/D) are increased, the bearing strength reaches higher values. At low values of W/D, the failure types are net-tension or shear-out which are weak type of failure, and high values of W/D, the failure type is bearing which is better mode of resisting load. While the W/D ratio is 2, net tension mode occurs. The bearing strengths are very similar to each other for specimens of W/D>3.

When the E/D ratio is 4 and 5,the bearing strength is close to each other and the failure mode is bearing which is the best mode of resisting load. When E/D=1 the bearing strength is small and failure mode is shear out or net tension which is the weakest mode. In spite of failure occurs, loading goes on with the effect of K/D ratio. In addition, the failure types are bearing or shear-out for specimens of K/D>3, when the W/D>2 .

In net-tension and shear-out failure, the reduction in load is both greater and more sudden. But in bearing failure, load does not drop suddenly. Therefore, joints that fail in bearing mode are stronger and safer joints.

REFERENCES

Aktaş, A, & Karakuzu, R. (1999). Failure Analysis of Two-Dimensional Carbon-Epoxy Composite Plate Pinned Joint. *Mechanics of Composite Materials and Structures*, *6*, 347-361.

Bathe, K.J. (1996). *Finite Element Procedures in Engineering Analysis.* Prentice-Hall Inc. Englewood Cliffs, New Jersey.

Camanho, P.P., & Matthews, F.L. (1997). Stress analysis and strength prediction of mechanically fastened joints in FRP: a review. *Composites Part A, 28A*, 529-47.

Camanho, P.P, & Matthews, F.L. (1999). A Progressive Damage Model for Mechanically Fastened Joints in Composite Laminates. *Journal of Composite Materials*, *33*, 2248-2280

Chandrupatla, T.R., & Belengundu, A.D. (1991). *Introduction to Finite Elements in Engineering.* Prentice-Hall.

Chang, F.K., Scott, R.A., & Springer, G.S. (1982). Strength of Mechanically Fastened Composite Joints. *Journal of Composite Materials*, *16*, 470-494.

Chang, F.K., Scott, R.A., & Springer, G.S. (1984)a. Failure of Composite Laminates Containing Pin Loaded Holes- Method and Solution. *Journal of Composite Materials*, *18*, 255-278

Chang, F.K., Scott, R.A., & Springer, G.S. (1984)b. Failure Strength of Nonlinearly Elastic Composite Laminates Containing a Pin Loaded Hole. *Journal of Composite Materials*, *18*, 464-477

Chang, F.K. (1986). The Effect of Pin Load Distribution on the Strength of Pin Loaded Holes in Laminated Composites. *Journal of Composite Materials*, *20*, 401-408

Dano, M.L., Gendron, G., & Piccard, A. (2000). Stress and Failure Analysis of Mechanically Fastened Joints in Composite Laminates. *Composite Structures*, *50*, 287-296.

Godwin, E.W., & Matthews, F.L. (1980, July). A review of the strength of joints in fibre-reinforced plastics. *Composites*, 155-160.

Gülem, T., & Icten, B.M. (2004). Failure Analysis of Woven Laminated Glass-vinylester Composites with Pin-loaded Hole. *Composite Structures*, (In Press).

Hamada, H., & Maekawa, Z.I. (1996). Strength Prediction of Mechanically Fastened Quasi-Isotropic Carbon/Epoxy Joints. *Journal of Composite Materials*, *30*, 1596-1612.

Hassan, N.K., Mohamedien, M.A., & Rizkalla, S.H. (1996). Finite element analysis of bolted connections for PFRP composites. *Composites: Part B, 27B*, 339-349.

Hung, C.L., & Chang, F.K. (1996). Bearing Failure of Bolted Composite Joints. Part II: Model and Verification. *Journal of Composite Materials*, *30*, 1359-1400.

Jones, R. M. (1999). *Mechanics of Composite Material. (2th ed.).* Tokyo: Taylor& Francis.

Icten, B.M., & Karakuzu, R. (2002). Progressive failure analysis of pin loaded carbon-epoxy woven composite plates. *Composite Science and Technology*, *62*, 1259-1271.

Icten, B.M., Okutan, B., & Karakuzu, R. (2003). Failure strength of Woven Glass Fiber-epoxy Composites Pinned Joints. *Journal of Composite Materials*, *37*, 1337-1351.

Icten, B.M., & Sayman, O., (2003). Failure analysis of pin-loaded aluminium-glass-epoxy sandwich composite plates. *Composite Science and Technology*, *63*, 727-737

Kim, S.J., & Kim, J.H. (1995). Finite element analysis of laminated composite plates with multi-pin joints considering friction. *Computers and Structures*, *55*, No:3, 507-514.

Kim, S.J., Hwang, J.S., & Kim, J.H. (1998, January). Progressive failure analysis of pin-loaded laminated composites using penalty finite element method. *AIAA Journal*, *36*, No: 1, 75-80.

Kretsis, G., & Matthews, F.L. (1985, April). The strength of bolted joints in glass fibre/epoxy laminates. *Journal of Composite Materials*, 16, 92-102

Lessard, L.B., & Shokrieh, M.M. (1995). Two-Dimensional Modelling of Composite Pinned-Joint Failure. *Journal of Composite Materials*, 29, 671-697.

McCarthy, C.T., McCarthy, M.A., & Lawlor, V.P. (2005). Progressive damage analysis of multi-bolt composite joints with variable bolt-hole clearances. *Composites: Part B, 36B*, 290-305.

Okutan, B., Aslan, Z., & Karakuzu, R. (2001). A Study of The Effects of Various Geometric Parameters On The Failure Strength of Pin-Loaded Woven-Glass-Fiber Reinforced Epoxy Laminate. *Composite Science and Technology*, *61*, 1491-1497.

Pierron, F., & Cerisier, F. (2000). A Numerical and Experimental Study of Woven Composite Pin-Joints. *Journal of Composite Materials*, *34*, 1028-1054.

Reddy, J.N. (1997). *Mechanics of Laminated Composite Plates.* Boca Raton: CRC Press.

Wang, H.S., Hung, C.L., & Chang, F.K. (1996). Bearing Failure of Bolted Composite Joints. Part I: Experimental Characterization. *Journal of Composite Materials, 30*, 1284-1313